

Controls on nitrite oxidation in the upper Southern Ocean: insights from winter kinetics experiments in the Indian sector

Mhlangabezi Mduyana^{1,2*}, Tanya Marshall¹, Xin Sun^{3,4}, Jessica M. Burger¹, Sandy J. Thomalla^{2,5}, Bess B. Ward³ and Sarah E. Fawcett^{1,5}

¹Department of Oceanography, University of Cape Town, Rondebosch, South Africa

²Southern Ocean Carbon and Climate Observatory (SOCCO), CSIR, Rosebank, South Africa

³Department of Geosciences, Princeton University, Princeton, New Jersey, USA

⁴Department of Ecology and Evolutionary Biology, Yale University, New Haven, Connecticut, USA

⁵Marine and Antarctic Research centre on Innovation and Sustainability (MARIS), University of Cape Town, Rondebosch, Cape Town, South Africa

*Corresponding author: M. Mduyana, mdtmhl001@myuct.ac.za

Abstract

Across the Southern Ocean in winter, nitrification is the dominant mixed-layer nitrogen cycle process, with some of the nitrate produced therefrom persisting to fuel productivity during the subsequent growing season. [Because this nitrate constitutes a regenerated rather than a new nutrient source to phytoplankton, it will not support net removal of atmospheric CO₂.](#) To better understand the controls on Southern Ocean nitrification, we conducted nitrite oxidation kinetics experiments in surface waters across the western Indian sector in winter. While all experiments (seven in total) yielded a Michaelis-Menten relationship with substrate concentration, the nitrite oxidation rates only increased substantially once the nitrite concentration exceeded 115 ± 2.3 to 245 ± 18 nM, suggesting that nitrite oxidizing bacteria (NOB) require a minimum (i.e., “threshold”) nitrite concentration to produce nitrate. The half-saturation constant [for nitrite oxidation](#) ranged from 134 ± 8 to 403 ± 24 nM, indicating a relatively high affinity of Southern Ocean NOB for nitrite, in contrast to results from culture experiments. Despite the high affinity of NOB for nitrite, its concentration rarely declines below 150 nM in the Southern Ocean’s mixed layer, regardless of season. In the upper mixed layer, we measured ammonium oxidation rates that were two- to seven-fold higher than the coincident rates of nitrite oxidation, indicating that nitrite oxidation is the rate-limiting step for nitrification in the winter Southern Ocean. The decoupling of ammonium and nitrite oxidation, combined with a possible nitrite concentration threshold for NOB, may explain the non-zero nitrite that persists throughout the Southern Ocean’s mixed layer year-round. [Additionally, nitrite oxidation may be limited by dissolved iron, the availability of which is low across the upper Southern Ocean. Our findings have implications for understanding the controls on nitrification and ammonium and nitrite distributions, both in the Southern Ocean and elsewhere.](#)

Deleted: .

Deleted: Because this nitrate constitutes a regenerated rather than a new nutrient source to phytoplankton, it will in net support no removal of atmospheric

Deleted: for nitrite oxidation

Deleted: Additionally, may be, the availability of which is low across the upper Southern Ocean Our findings have implications for understanding the controls on nitrification and ammonium and nitrite distributions, both in the Southern Ocean and elsewhere We hypothesize that the apparent threshold nitrite requirement of NOB indicates nitrite undersaturation of the heme-rich nitrite oxidoreductase enzyme, perhaps driven by the limited availability of iron in surface waters.

51 1. Introduction

52

53 The cycling of nitrogen (N) in the upper ocean is central to the role that phytoplankton and bacteria play
54 in atmospheric carbon dioxide (CO₂) consumption and production. Annually, the Southern Ocean
55 accounts for ~35% of total oceanic CO₂ removal (DeVries et al., 2017; Gruber et al., 2019; Watson et
56 al., 2020) and absorbs ~40% of anthropogenic CO₂ (Khatiwala et al., 2009; Hauck et al., 2015; Gruber
57 et al., 2019; Watson et al., 2020). The contribution of biology to CO₂ drawdown can be evaluated using
58 the new production paradigm, among other approaches. This framework defines phytoplankton growth
59 on nitrate (NO₃⁻) supplied from below the euphotic zone as “new production” and phytoplankton growth
60 on ammonium (NH₄⁺) recycled within the euphotic zone as “regenerated production” (Dugdale and
61 Goering 1967). Over appropriate timescales, new production is equivalent to “export production”, the
62 latter referring to the organic matter produced by phytoplankton that escapes recycling in surface waters
63 and sinks into the ocean interior, thereby sequestering atmospheric CO₂ at depth (Dugdale and Goering,
64 1967; Eppley and Peterson, 1979; Volk and Hoffert, 1985; Raven and Falkowski, 1999). The occurrence
65 of nitrification in the euphotic zone, which produces regenerated NO₃⁻, complicates applications of the
66 new production paradigm since phytoplankton growth fuelled by this NO₃⁻ will drive no net removal of
67 CO₂ (Yool et al., 2007).

68

69 In the Southern Ocean, nitrification appears to be largely confined to the dark waters below the euphotic
70 zone during the summertime period of maximum NO₃⁻ consumption by phytoplankton (DiFiore et al.,
71 2009; Mduyana et al., 2020). By contrast, the Southern Ocean winter is characterized by elevated
72 mixed-layer nitrification [rates](#), coincident with low rates of NO₃⁻ uptake (Smart et al., 2015; Mduyana
73 et al., 2020). Some of the NO₃⁻ regenerated in the winter mixed layer will be supplied to phytoplankton
74 during the proceeding spring and summer growing season, with negative implications for CO₂ removal
75 on an annual basis. That said, there is evidence that ammonia oxidizing archaea, the organisms that are
76 dominantly responsible for NH₄⁺ oxidation (the first step in the nitrification pathway) (Beman et al.,
77 2008; Newell et al., 2011; Peng et al., 2016) have a high iron requirement (Shafiee et al., 2019), such
78 that NH₄⁺ oxidation may at times experience iron limitation ([Mduyana et al. 2022](#)). If this limitation
79 is verified and proves widespread in the environment, one implication is that the iron-deplete conditions
80 of the surface Southern Ocean may restrict mixed-layer nitrification and by extension, [decrease the](#)
81 [extent to which phytoplankton growth is fueled by regenerated nitrate](#).

82

83 Nitrification is a chemoautotrophic process involving two pathways usually facilitated by different
84 groups of microorganisms. The first step is NH₄⁺ oxidation, which involves the oxidation of NH₄⁺ via
85 hydroxylamine and nitric oxide to NO₂⁻ (Walker et al. 2010; Vajjala et al. 2013; Kozłowski et al. 2016;
86 Caranto and Lancaster 2017) by ammonia oxidizing archaea and bacteria (AOA and AOB, respectively;
87 collectively, ammonia oxidizing organisms, AOO). The second step is the oxidation of NO₂⁻ to NO₃⁻ by

Deleted: -

Deleted: -

Deleted: -

Deleted: -

Deleted:

Deleted: rates

Deleted: decrease the extent to which phytoplankton growth is fueled by regenerated nitrate.

96 nitrite oxidizing bacteria (NOB), a polyphyletic group of microbes that is not well-understood in the
97 ocean (Watson et al., 1986; Beman et al., 2013; Daims et al., 2016; Pachiadaki et al., 2017; Sun et al.,
98 2021). In general, NO_2^- oxidation rate data are limited, with few measurements available for the
99 Southern Ocean (Bianchi et al. 1997; Mdotyana et al. 2020; Olson 1981a). Such measurements are
100 critical, however, if we are to better understand the controls on nitrification in the Southern Ocean
101 mixed layer and the connection between NO_3^- production by NOB and its subsequent removal by
102 phytoplankton.

103

104 One approach for investigating the controls on NO_2^- oxidation is through experiments designed to yield
105 a hyperbolic Michaelis-Menten relationship between NO_2^- oxidation rate and NO_2^- concentration.
106 Useful kinetic parameters can be derived from this relationship, such as the maximum oxidation rate
107 (V_{max}) and the half-saturation constant (K_m), with the latter indicating the NO_2^- concentration at which
108 the oxidation rate equals $V_{\text{max}}/2$. Estimates of K_m provide information regarding the efficiency of NOB
109 in acquiring substrate NO_2^- , with a lower K_m indicating a higher affinity for NO_2^- , while V_{max} denotes
110 the maximum rate of NO_2^- oxidation that can be achieved under a [given](#) set of conditions by a particular
111 NOB community. In the ocean, direct measurements of NO_2^- oxidation kinetic parameters are extremely
112 limited (Olson, 1981; Sun et al., 2017, 2021; Zhang et al., 2020), with no estimates available for the
113 Southern Ocean. K_m values derived from culture studies of NOB range from 9-544 μM (Nowka et al.,
114 2015; Ushiki et al., 2017), orders of magnitude higher than the existing estimates for natural
115 assemblages of NOB in coastal waters and oxygen deficient zones (ranging from 0.07-0.51 μM ; Olson,
116 1981; Sun et al., 2017; Zhang et al., 2020). This discrepancy emphasizes the gaps in our understanding
117 of NO_2^- oxidation and the organisms that catalyse it.

118

119 Generally, NO_2^- concentrations in the low-latitude oxygenated ocean reach a maximum near the base
120 of the [euphotic zone](#) (i.e., the primary nitrite maximum; PNM), with much lower concentrations above
121 and below this depth (Lomas and Lipschultz 2006). By contrast, at higher latitudes including in the
122 Southern Ocean, the NO_2^- concentrations are elevated (100-400 nM) and fairly invariant throughout the
123 mixed layer in all seasons (Zakem et al. 2018; Fripiat et al. 2019; Mdotyana et al. 2020). A possible
124 explanation for this NO_2^- accumulation is a decoupling of the NH_4^+ and NO_2^- oxidation rates, with NO_2^-
125 oxidation being the rate-limiting step in the nitrification pathway, contrary to expectations for
126 oxygenated marine waters (Kendall, 1998; Walker et al., 2010; Vajrjala et al., 2013). However, this idea
127 has yet to be examined using observations.

128

129 To better understand the controls on NO_2^- oxidation (and thus, nitrification) in the Southern Ocean, we
130 conducted a series of NO_2^- oxidation kinetics experiments in wintertime surface waters across the
131 western Indian sector. At every station (seven in total) along a transect between the Subtropical and
132 Marginal Ice Zones, NO_2^- oxidation rates increased with increasing NO_2^- concentrations, as per the

Deleted: given

Deleted: mixed layer

135 expected Michaelis-Menten relationship. The derived K_m values were low and increased with increasing
 136 ambient NO_2^- . Additionally, there appeared to be a minimum NO_2^- concentration that was required
 137 before the NO_2^- oxidation rates increased significantly, implying a “threshold” NO_2^- requirement ~~for~~
 138 NO_2^- ~~oxidation in the Southern Ocean~~. Finally, coincident measurements of euphotic zone NH_4^+ and
 139 NO_2^- oxidation rates suggest that NO_2^- oxidation is rate-limiting for nitrification across the Southern
 140 Ocean in winter.

142 2. Materials and Methods

144 2.1. Sampling site and experimental design

145 A winter cruise was undertaken onboard the R/V *SA Agulhas II* in July 2017 between Cape Town, South
 146 Africa, and the Marginal Ice Zone (MIZ; encountered at 61.7°S; de Jong et al., 2018), returning to South
 147 Africa along the meridional WOCE I06 transect (30°E) (Figure 1). Sampling was conducted on two
 148 legs – between 37°S and 62°S on the southward leg (Leg 1) and between 59°S and 41°S on the
 149 northward ~~return~~ leg along the WOCE I06 line (Leg 2). During Leg 1, only surface samples were
 150 collected while on Leg 2, the deployment of conductivity-temperature-depth (CTD) hydrocasts allowed
 151 for depth-profile sampling.

152
 153 *2.1.1 Hydrography and nutrient collections:* The positions of the major hydrographic fronts (the
 154 Subtropical Front, STF; Subantarctic Front, SAF; Polar Front, PF; and Southern Antarctic Circumpolar
 155 Current Front, SACCF; Figure 1) were determined from temperature and salinity measured by the ship’s
 156 hull-mounted thermosalinograph (~7 m), augmented by temperature, salinity, and oxygen
 157 concentrations measured on Leg 2 by the CTD sensors (Orsi et al., 1995; Belkin and Gordon, 1996;
 158 Pollard et al., 2002; Read et al., 2002). For the hydrocast stations, the mixed layer depth was determined
 159 for each CTD (up)cast as the depth between 10 m and 400 m of maximum Brunt Väisälä frequency
 160 squared (i.e., N^2) (Schofield et al., 2015; Carvalho et al., 2017). ~~Surface photosynthetically active~~
 161 ~~radiation (PAR) was not measured continuously during the cruise; we thus use latitude as a qualitative~~
 162 ~~proxy for light availability during Leg 1.~~

163
 164
 165 *2.1.2 Nutrient samples:* Seawater samples were collected every four hours from the ship’s underway
 166 system (~7 m intake) on Leg 1 for the determination of NO_2^- concentrations (Figure 1a). During Leg 2,
 167 samples were collected from Niskin bottles fired remotely between the surface and 500 m at eight
 168 hydrocast stations for the analysis of NO_2^- , NO_3^- , and NH_4^+ concentrations (see Figure 1b and c for
 169 station locations and sampling depths). For NO_2^- and NO_3^- , unfiltered seawater was collected in
 170 duplicate 50 mL polypropylene centrifuge tubes that were analysed shipboard within 24 hours of
 171 collection (NO_2^-) or stored frozen at -20°C until analysis (NO_3^-). Seawater samples for NH_4^+ were

Deleted: for

Deleted: oxidation in the Southern Ocean

Deleted: return

Deleted: continuously thus a qualitative availability during Leg 1...

177 collected unfiltered in duplicate high-density polyethylene (HDPE) bottles that had been “aged” with
178 orthophthaldialdehyde (OPA) working reagent, and analysed shipboard within 24 hours of collection.

179

180 *2.1.3 NO₂⁻ oxidation kinetics experiments:* On Leg 1, seawater samples were collected from the surface
181 via the ship’s underway system at seven stations spanning the different zones of the Southern Ocean
182 (the Subtropical Zone (STZ) to the north of the STF, at the STF, the Subantarctic Zone (SAZ) between
183 the STF and SAF, the Polar Frontal Zone (PFZ) between the SAF and PF, the Open Antarctic Zone
184 (OAZ) between the PF and SACCF, and the Marginal Ice Zone (MIZ) south of the SACCF; St 01 to St
185 07 in Figure 1a). At each station, 25 L of seawater were collected in a single carboy that was gently
186 shaken to homogenize the contents before the seawater was filtered through a 200 µm nylon mesh to
187 remove zooplankton grazers and then dispensed into 250 mL acid-washed opaque HDPE bottles. All
188 the bottles were rinsed three times with sample water prior to filling. Eight sets of duplicate 250 mL
189 bottles were amended with Na¹⁵NO₂ to yield ¹⁵NO₂⁻ concentrations ranging from 10 nM to 1500 nM.

190

191 *2.1.4 Depth distribution of NO₂⁻ oxidation:* On Leg 2, seawater was collected at four stations (one each
192 in the Polar Antarctic Zone (PAZ; just north of the edge of the MIZ), OAZ, PFZ, and SAZ; St 08 to St
193 11 in Figure 1a-c) using a CTD-rosette equipped with 24 12-L Niskin bottles. Seawater from six depths
194 (10 m, 25 m, 50 m, 75 m, 200 m, and 500 m) was pre-filtered (200 µm nylon mesh) and transferred into
195 rinsed 250 mL acid-washed opaque HDPE bottles. Duplicate bottles from each depth were amended
196 with Na¹⁵NO₂ to yield a final ¹⁵NO₂⁻ concentration of 200 nM. From all incubation bottles (for kinetics
197 and depth-profile experiments), initial (T₀) subsamples were collected in 50 mL centrifuge tubes
198 immediately after the addition of ¹⁵NO₂⁻. The opaque HDPE bottles from the upper 75 m were then
199 incubated in custom-built on-deck incubators supplied with running surface seawater, while those from
200 200 m and 500 m were incubated in a ~2°C cold room. The incubations lasted 23-30 hours and were
201 terminated via the collection of final (T_f) subsamples (50 mL). Subsamples were filtered (0.2 µm) and
202 stored frozen at -20°C until analysis.

203

204 *2.1.5 Depth distribution of NO₃⁻ uptake:* To assess the extent to which mixed-layer NO₂⁻ oxidation
205 supports wintertime NO₃⁻ uptake by phytoplankton, we also conducted NO₃⁻ uptake experiments over
206 the upper 75 m (the approximate depth of the euphotic zone) at St 08 to St 11 on Leg 2. Seawater was
207 collected from four depths – 10 m, 25 m, 50 m, and 75 m – in duplicate 2 L clear polycarbonate bottles
208 following filtration (200 µm nylon mesh) to remove large zooplankton grazers. Na¹⁵NO₃ was added to
209 each bottle to yield a final ¹⁵NO₃⁻ concentration of 3 µM, and the bottles were then transferred to custom-
210 built deck-board incubators equipped with neutral density screens that allowed for the penetration of
211 55%, 30%, 10%, and 1% of surface PAR. The bottles were kept at near *in situ* temperature via a supply
212 of continuously-running seawater from the underway system. Samples were incubated for 3-6 hours,
213 and incubations were terminated by filtering the bottle contents through pre-combusted (450°C for 8

Deleted: opaque

Deleted: large

216 hours) 0.3 µm glass fibre filters (GF-75; Sterlitech) that were subsequently enclosed in foil envelops
217 (pre-combusted at 500°C for 5 hours) [and](#) stored at -80°C until analysis.

Deleted: and

219 2.2. Laboratory analyses

220 2.2.1 *Nutrient concentrations*: Samples were analysed [shipboard](#) for NO₂⁻ concentrations using the
221 colorimetric method of Grasshoff et al., (1983) and a Thermo Scientific Genesys 30 Visible
222 spectrophotometer (detection limit of 20 nM, precision of ±20 nM). NO₃⁻+NO₂⁻ concentrations were
223 measured ashore using a Lachat Quick-Chem flow injection autoanalyzer (Egan, 2008) in a
224 configuration with a detection limit of 0.2 µM and precision of ±0.3 µM. The concentration of NO₃⁻
225 was determined by subtracting NO₂⁻ from NO₃⁻+NO₂⁻. Aliquots of a certified reference material
226 (JAMSTEC) were included in each NO₂⁻ and NO₃⁻+NO₂⁻ run to ensure measurement accuracy. The
227 NH₄⁺ concentrations were also determined shipboard using the fluorometric method of Holmes et al.
228 (1999); the methodological details and NH₄⁺ data are discussed at length in (Mdutyana 2021) [and \(Smith](#)
229 [et al., \(2022\).](#)

Deleted: shipboard

Deleted:

231 2.2.2 *NO₂⁻ oxidation rates*: Using the denitrifier-isotope ratio mass spectrometer (IRMS) method
232 (Sigman et al., 2001; [Weigand et al., 2016](#)), we measured the δ¹⁵N of NO₃⁻ (δ¹⁵N-NO₃⁻) produced from
233 ¹⁵NO₂⁻ oxidation for both the kinetics and depth-profile experiments (δ¹⁵N, in ‰ vs. air, =
234 (¹⁵N/¹⁴N_{sample}/¹⁵N/¹⁴N_{air} - 1) × 1000). Samples were measured using a Delta V Plus IRMS with a custom-
235 built purge-and-trap front end ([Weigand et al., 2016](#)) in a configuration with a detection limit of 0.2
236 nmol of N and a δ¹⁵N precision of 0.2‰. Prior to isotope analysis, samples were treated with sulfamic
237 acid (15 mM) to remove ¹⁵NO₂⁻ remaining at the end of the experiments, after which sample pH was
238 adjusted to ~7-8 via the addition of 2 M NaOH. To account for inefficiencies in ¹⁵NO₂⁻ removal, both
239 the T_f and T₀ samples were treated with sulfamic acid [prior to analysis of](#) δ¹⁵N-NO₃⁻ (more accurately,
240 δ¹⁵N-NO₃⁻+NO₂⁻), with the difference between them taken as the ¹⁵NO₃⁻ enrichment due to ¹⁵NO₂⁻
241 oxidation (Peng et al., 2015). International reference materials (IAEA-N3, USGS 34, USGS 32) were
242 used to calibrate the measured δ¹⁵N-NO₃⁻.

Deleted: Weigand et al. 2016)

Deleted: Weigand et al. 2016

Deleted: prior to analysis for of

244 The rate of NO₂⁻ oxidation (NO₂⁻_{ox}; nM d⁻¹) was calculated following Peng et al., (2015) as:

$$246 \quad \text{NO}_2^-_{\text{ox}} = \frac{\Delta[^{15}\text{NO}_3^-]}{f_{\text{NO}_2^-}^{15} \times T} \quad (1)$$

247
248 Where Δ[¹⁵NO₃⁻] is the change in the concentration of ¹⁵NO₃⁻ between the start and end of the incubation
249 due to NO₂⁻ oxidation, calculated from the difference in the measured δ¹⁵N-NO₃⁻ between the T_f and T₀
250 samples, f_{NO₂⁻}¹⁵ is the fraction of the NO₂⁻ substrate pool labelled with ¹⁵N at the start of the incubation,

calculated following the direct measurement of ambient NO_2^- concentration, and T is the incubation length (days). Detection limits for NO_2^- rates ranged from 0.11 to 0.36 nM d^{-1} , calculated according to Santoro et al. (2013) and Mdutyana et al. (2020).

2.2.3 Kinetic model: Kinetic parameters are typically calculated using the Michaelis-Menten (MM) equation for enzyme kinetics (Monod, 1942):

$$V = \frac{V_{\max} \times S}{K_m + S} \quad (2)$$

where V is the measured reaction rate, V_{\max} is the maximum reaction rate achievable under *in situ* conditions at saturating substrate (S) concentrations, and K_m is the half-saturation constant, defined as the substrate concentration at which $V = V_{\max}/2$.

The MM equation (equation 2) is a rectangular hyperbola, meaning that the asymptotes along the x- and y-axes are perpendicular. By definition, when S (the x-axis variable) is equal to zero, V (the y-axis variable) is also zero, forcing the model through the origin (0,0). In the case of NO_2^- oxidation, the assumption that once $S > 0$, $V > 0$ is appropriate in waters where the ambient NO_2^- concentration is near-zero or where NO_2^- is non-zero but considerably lower than the K_m . In the Southern Ocean, mixed-layer NO_2^- concentrations are typically $\geq 150 \text{ nM}$ (Cavagna et al., 2015; Zakem et al., 2018; Fripiat et al., 2019; Mdutyana et al., 2020) and forcing the MM model through the origin results in a poor fit to the measurements (red line in Figure S1). This poor fit, in turn, leads to clearly inaccurate estimates of the kinetic parameters, particularly K_m (Table S1).

While not typical for studies of NO_2^- oxidation kinetics in the ocean, the standard form of non-linear regression models, including the MM equation, can be modified to better fit the observations (e.g., Birch, 1999; Tsoularis and Wallace, 2002; Archontoulis and Miguez, 2014). For application to our dataset, we modified equation 2 to allow $V = 0$ at $S > 0$ by subtracting a location parameter, C, from S (Figure 2) (Archontoulis and Miguez, 2014). In other words, we set the y-intercept (i.e., where $V = 0$) equal to C rather than to zero, which yields equation 3:

$$V = \frac{V_{\max} \times (S-C)}{K_m^* + (S-C)} \quad (3)$$

Using a non-linear, least-squares optimization method (Scipy lmfit package, Python 3.7.6), we solved equation 3 for V_{\max} , K_m^* , and C. The value of K_m^* derived in this way is relative to C, such that the substrate concentration at which $V = V_{\max}/2$ (i.e., K_m) is actually equal to $K_m^* + C$ (Supplemental Information). Mechanistically, C represents a “threshold” substrate concentration; when $S \leq C$, $V = 0$.

Deleted: calculated following the direct measurement of ambient NO_2^- concentration,

Deleted: the

Deleted:)

Deleted: (

Deleted: in this way

299 All [derived](#) kinetic parameters are reported as the best fit plus 95% confidence interval (i.e., mean $\pm 2\sigma$;
300 Table 1).

Deleted: derived

301
302 2.2.4 Revising the depth distribution of NO_2^- oxidation using K_m : For the NO_2^- oxidation experiments
303 conducted at the Leg 2 hydrocast stations (i.e., depth-profile experiments; St 08 to St 11), the $\text{Na}^{15}\text{NO}_2^-$
304 was added to yield a final $^{15}\text{NO}_2^-$ concentration of 200 nM at all the sampled depths. However, at low
305 ambient NO_2^- concentrations ($<1\text{-}2\text{ }\mu\text{M}$), an amendment of this magnitude may stimulate NO_2^-
306 oxidation, leading to an overestimation of the [in-situ](#) rates. We thus revised our measured NO_2^- rates
307 using the derived K_m values as per Rees et al. (1999), Diaz and Raimbault, (2000), and Horak et al.
308 (2013):

Deleted: in-situ

309
310
$$\text{corrNO}_2^-_{\text{ox}} = \frac{\text{NO}_2^-_{\text{ox}}}{\frac{[\text{NO}_2^-]_{\text{total}}}{K_m + [\text{NO}_2^-]_{\text{total}}} \times \frac{K_m + [\text{NO}_2^-]_{\text{amb}}}{[\text{NO}_2^-]_{\text{amb}}}} \quad (4)$$

311
312 Here, $\text{corrNO}_2^-_{\text{ox}}$ is the revised rate of NO_2^- oxidation, $\text{NO}_2^-_{\text{ox}}$ is the measured NO_2^- oxidation rate (equation 1),
313 $[\text{NO}_2^-]_{\text{amb}}$ is the ambient NO_2^- concentration measured at each depth, $[\text{NO}_2^-]_{\text{total}}$ refers to the
314 [concentration of](#) $^{15}\text{NO}_2^-$ [plus](#) $\text{NO}_2^-_{\text{amb}}$, and K_m is the derived half-saturation constant. We estimated
315 a K_m for each sample depth from the equation resulting from the linear regression of all derived K_m
316 values on $[\text{NO}_2^-]_{\text{amb}}$ (see section 4.2 below). We also computed $\text{corrNO}_2^-_{\text{ox}}$ using the K_m derived from
317 the Leg 1 kinetics experiment located nearest each hydrocast station, which yielded very similar results.
318 The values of $\text{corrNO}_2^-_{\text{ox}}$ presented here were computed using the K_m values derived from the linear
319 regression equation. Rates of NH_4^+ oxidation measured coincident with $\text{NO}_2^-_{\text{ox}}$ on Leg 2 (see [M-dutyana](#)
320 [et al., 2022](#), were similarly revised (to yield $\text{corrNH}_4^+_{\text{ox}}$) using the K_m values derived from kinetics
321 experiments conducted during Leg 1 [of the cruise](#) – for St 08 and 09, $K_m = 137\text{ nM}$, for St 09, $K_m = 67$
322 nM, and for St 11, $K_m = 28\text{ nM}$.

Deleted: concentration of

Deleted: plus

Deleted: (

Deleted:)

Deleted: M-dutyana et al. 2022)

Deleted: of the cruise

323
324 2.2.5 Isotopic dilution of $^{15}\text{NO}_2^-$ by co-occurring NH_4^+ oxidation: The focus of this study is the second
325 step in the nitrification pathway. However, not only will NO_2^- have been consumed in our incubation
326 bottles (i.e., oxidized to NO_3^-), but it will also have been produced by NH_4^+ oxidation, the first step in
327 the nitrification pathway. For all of our NO_2^- oxidation rate experiments (kinetics and depth-profile),
328 we measured the coincident rates of NH_4^+ oxidation ([M-dutyana et al., 2022](#)), and these data can be used
329 to account for any dilution of the $^{15}\text{NO}_2^-$ pool by $^{14}\text{NO}_2^-$ produced from $^{14}\text{NH}_4^+$ oxidation (following the
330 approach of [Glibert et al. \(1982, 1985\)](#) and [Mulholland and Bernhardt \(2005\)](#)). We found that isotopic
331 dilution in the mixed layer was minor because the ambient NO_2^- concentrations were reasonably high
332 (mean of $157 \pm 54\text{ nM}$, range of 64 to 226 nM for all the depths at which experiments were conducted;
333 Figure 1a-b) and the NH_4^+ oxidation rates were fairly low (mean of $13.4 \pm 4.0\text{ nM d}^{-1}$, range of 7.8 to
334 22.0 nM d^{-1} ; see Figure 3f-j for the depth profile rates and [M-dutyana et al., \(2022\)](#) for the kinetics station

Deleted: M-dutyana et al. 2022

Deleted: (

Deleted:) and

Deleted: (

Deleted:)

Field Code Changed

Deleted: et al. (2022)

rates). Below the mixed layer where the ambient NO_2^- concentrations were near-zero, so too were the NH_4^+ oxidation rates, which again resulted in minimal dilution of the $^{15}\text{NO}_2^-$ pool. Accounting for isotope dilution increased the NO_2^- oxidation rates by 0 to 12% (mean of $3.9 \pm 0.3\%$ and median of $3.7 \pm 0.3\%$), which is within the experimental error associated with the rate measurements; we thus consider the effect of isotope dilution to be negligible

2.2.6 Nitrate uptake rates: On shore, the GF-75 filters were oven-dried at 45°C for 24 hours, then pelletized into tin cups following the removal of unused peripheral filter. The concentration and isotopic composition of the particulate organic N (PON) captured on the filters was analyzed using a Delta V Plus IRMS coupled to a Flash 2000 elemental analyser, with a detection limit of $1 \mu\text{g N}$ and precision of $\pm 0.005 \text{ At\%}$. Blanks (combusted unused filters + tin capsules) and laboratory running standards calibrated to international reference materials were run after every five to ten samples. The absolute rates of NO_3^- uptake (ρNO_3^- ; nM d^{-1}) were calculated after blank correction according to the equations of Dugdale and Wilkerson (1986) assuming a day-length of between 7 and 10 hours, depending on the station latitude. To compute the fraction of the mixed-layer NO_3^- pool consumed by phytoplankton that derived from *in situ* nitrification, we trapezoidally-integrated ρNO_3^- and $\text{corrNO}_2^-_{\text{ox}}$ over the mixed layer following Mdutyana et al., (2020), and then divided the integrated values of $\text{corrNO}_2^-_{\text{ox}}$ by ρNO_3^- .

3. Results

3.1 Hydrography and nutrient concentrations

The positions of the major hydrographic fronts during both legs of the cruise are shown in Figure 1a. At the hydrocast stations (Leg 2), the mixed layer depth (MLD) averaged 143 m in the OAZ, 146 m in the PFZ, 205 m in the SAZ, and 113 m in the STZ, which is within the reported climatological range for the western Indian sector of the Southern Ocean in winter (Sallée et al. 2010). Underway ambient NO_2^- concentrations (Leg 1) ranged from 74 nM to 232 nM (transect average of $168 \pm 48 \text{ nM}$, median of 177 nM) and generally increased with latitude, albeit with a high degree of variability (Figure 1a; Figure S2). The ambient NO_2^- concentrations at the hydrocast stations were fairly constant throughout the mixed layer (ranging from $55 \pm 35 \text{ nM}$ to $159 \pm 73 \text{ nM}$), decreasing rapidly to values below detection by 150-200 m (Figure 1b). Mixed-layer NO_2^- showed no clear latitudinal trend, mainly because of the anomalously low concentrations measured at St 09 (54°S ; mixed-layer average of $64 \pm 30 \text{ nM}$, compared to 144 ± 56 for the seven other hydrocast stations). The NO_3^- concentrations were also near-homogenous throughout the mixed layer, decreasing from an average of $28.4 \pm 0.2 \mu\text{M}$ at the southernmost station (St 08; 59°S) to $3.7 \pm 1.1 \mu\text{M}$ at the northernmost station (41°S), and increasing below the mixed layer as expected (Figure 1c).

3.2. NO_2^- oxidation rates

Deleted: of the Southern Ocean

387 3.2.1 *Kinetics experiments*: At all the kinetics stations (St 01 to St 07; Leg 1), an MM curve could be
 388 fit to the NO_2^- oxidation rate *versus* substrate concentration measurements using equation 3 (Figure 2).
 389 The derived kinetic parameters varied across the transect (Table 1). The maximum NO_2^- oxidation rate
 390 (V_{\max}) increased southwards from $5.2 \pm 0.1 \text{ nM d}^{-1}$ at the STF (St 02; Figure 2b) to $13 \pm 0.4 \text{ nM d}^{-1}$ in
 391 the AZ (St 05; Figure 2e), before decreasing in the MIZ to $8.2 \pm 0.1 \text{ nM d}^{-1}$ at St 06 (Figure 2f) and 6.6
 392 $\pm 0.3 \text{ nM}$ at St 07 (Figure 2g). The average V_{\max} for the transect was $9.0 \pm 1.1 \text{ nM d}^{-1}$. The half-saturation
 393 constant (K_m) increased from $134 \pm 8.0 \text{ nM}$ at the STF (St 02) to $403 \pm 24 \text{ nM}$ in the MIZ (St 06), with
 394 a transect average of $277 \pm 31 \text{ nM}$. The value of C showed a positive relationship with $[\text{NO}_2^-]_{\text{amb}}$ ($R^2 =$
 395 0.59 ; $p = 0.045$) and no strong relationship with latitude, and ranged from $115 \pm 2.3 \text{ nM}$ at the STF (St
 396 02) to $245 \pm 18 \text{ nM}$ in the A Z (St 05), with a transect average of $181 \pm 45 \text{ nM}$.

397
 398 3.2.2 *Depth-profile experiments*: NO_2^- oxidation rates at St 08 to St 11, calculated using equation 1,
 399 were low and largely invariant over the upper 75 m, ranging from 1.9 to 9.7 nM d^{-1} (average of $4.9 \pm$
 400 2.4 nM d^{-1} ; filled symbols in Figure 3b-e). All stations showed a maximum NO_2^- oxidation rate at 200
 401 m (roughly coincident with or just below the MLD), ranging between 11 and 28 nM d^{-1} (average of 18
 402 $\pm 7.0 \text{ nM d}^{-1}$). The NO_2^- oxidation rates showed a latitudinal gradient, with lower rates in the AZ (St 08
 403 and 09) than in the PFZ (St 10) and SAZ (St 11).

404
 405 Revising the NO_2^- oxidation rates using equation 4 decreased their 0-75 m values by 13 to 26% (i.e.,
 406 $\text{corrNO}_2^-_{\text{ox}}$ ranged from 1.6 to 8.5 nM d^{-1} and averaged $4.0 \pm 2.0 \text{ nM d}^{-1}$ over the upper 75 m; open
 407 symbols in Figure 3b-e). The largest decrease (of 39 to 68%) occurred at 200 m and 500 m, coinciding
 408 with the very low ambient NO_2^- concentrations (Figure 3a). Nonetheless, at all but St 08, the maximum
 409 NO_2^- oxidation rate was still observed at 200 m, although its magnitude was lower. The coincidentally-
 410 measured and revised NH_4^+ oxidation rates ($\text{corrNH}_4^+_{\text{ox}}$) showed a similar pattern, with the largest
 411 decrease occurring at the depths with the lowest ambient NH_4^+ concentrations (Figure 3f-j) – over the
 412 upper 75 m, the rates decreased by 1 to 9% at St 08 to St 10 where the mixed-layer NH_4^+ concentrations
 413 averaged 263 ± 4.3 to $655 \pm 15 \text{ nM}$, while at St 11 where the mixed-layer NH_4^+ concentration averaged
 414 $13 \pm 1.6 \text{ nM}$, the rates decreased by $40 \pm 23\%$. Similar to the NO_2^- oxidation rates, the NH_4^+ oxidation
 415 rates decreased most at 200 m and 500 m, by between 33% and 70%. Hereafter, we use the revised NO_2^-
 416 and NH_4^+ oxidation rates ($\text{corrNO}_2^-_{\text{ox}}$ and $\text{corrNH}_4^+_{\text{ox}}$, respectively) when referring to the depth
 417 distributions of these processes, including in Figures 5 and 6. We note, however, that the revised rates
 418 may still not be accurate since K_m was not derived individually for each depth at each station (Horak et
 419 al., 2013). Nonetheless, because of the high concentration of the ^{15}N -tracer amendments relative to all
 420 derived K_m values, we are confident that the revised rates are more representative of *in situ* conditions
 421 than the rates computed using equation 1.

422
 423 3.3 NO_3^- uptake rates

Formatted: Superscript

Formatted: Font: Italic

Deleted: MLD

Deleted: the

Deleted: . nonethelessNonetheless

Deleted: by

Field Code Changed

The rates of NO_3^- uptake (ρNO_3^-) were low and relatively homogenous over the upper 75 m at each station (Figure S3a). Average euphotic zone ρNO_3^- increased northwards, from $2.9 \pm 1.1 \text{ nM d}^{-1}$ at St 08 in the AZ to $12 \pm 2.0 \text{ nM d}^{-1}$ at St 11 in the SAZ, with a transect average of $6.2 \pm 3.4 \text{ nM d}^{-1}$. The euphotic zone PON concentrations also increased northwards, from $0.24 \pm 0.02 \text{ } \mu\text{M}$ at St 08 to $0.47 \pm 0.08 \text{ } \mu\text{M}$ at St 11 (Figure S3b). Integrated over the mixed layer, $\text{corrNO}_2^-_{\text{ox}}$ accounted for an average of 122% of ρNO_3^- (range of 63% at St 09 to 237% at St 08 in the AZ; Table S2), [consistent with previous observations from](#) the wintertime Southern Ocean (Mdutyana et al., 2020).

Deleted: consistent with previous observations from

4. Discussion

Across all the major zones of the wintertime Southern Ocean, the addition of NO_2^- to samples of surface seawater stimulated NO_2^- oxidation following a Michaelis-Menten relationship, suggesting that substrate availability plays a dominant role in determining the rate of NO_3^- production in the Southern Ocean's winter mixed layer. Curiously, however, we also observed an apparent minimum substrate requirement of NO_2^- oxidation (i.e., a "threshold" NO_2^- concentration, ranging from 115 to 245 nM), which [contradicts](#) expectations for a "classical" Michaelis-Menten relationship (i.e., V is [expected](#) to increase as soon as $S > 0$, assuming S is limiting to V ; Monod, 1942). Below, we examine our findings in the context of existing estimates of NO_2^- oxidation kinetic parameters and then evaluate the potential drivers of the trends that we observe. We also discuss possible reasons for the apparent requirement of Southern Ocean NOB for a threshold ambient NO_2^- concentration and consider the implications thereof for the regional N cycle.

Deleted: These data confirm that, at least in a mass balance sense, most of the mixed-layer NO_3^- consumed by phytoplankton in winter, and likely also a significant fraction assimilated in spring, supports regenerated rather than new production, thus weakening the biological CO_2 sink and complication the use of new production as a proxy for carbon export (Yool et al., 2007; Mdutyana et al., 2020).

Deleted: NO_2^- oxidation, the ultimate step in the nitrification pathway, is important in oceanic N cycling because it produces NO_3^- , the most oxidized and dominant form of N that controls phytoplankton growth across most of the global ocean (Moore et al., 2013). Experiments designed to measure the kinetics of NO_2^- oxidation, as conducted here, allow for an examination of the controls on marine nitrification.

Deleted: contradicts

Deleted: expected

4.1 Southern Ocean NO_2^- oxidation kinetic parameters in the context of existing estimates

Measurements of NO_2^- oxidation rates are limited in the Southern Ocean, with only two studies that have directly measured this pathway in open-ocean waters (Bianchi et al. 1997; Mdutyana et al. 2020). For NO_2^- oxidation kinetics, there are no data at all for the Southern Ocean. This scarcity of measurements is unsurprising given that *in situ* NO_2^- oxidation kinetics studies are generally limited; indeed, to our knowledge, there are only two studies from the coastal ocean (Olson 1981a; Zhang et al. 2020) and two from the Eastern Tropical North Pacific oxygen deficient zone (ETNP ODZ; with [these](#) experiments conducted across a range of ambient oxygen concentrations; Sun et al., 2017, 2021). By contrast, there exist numerous estimates of NO_2^- oxidation kinetic parameters determined using cultured marine NOB (e.g., Sorokin et al., 2012; Nowka et al., 2015; Jacob et al., 2017; Kits et al., 2017; Zhang et al., 2020). In general, culture experiments suggest far higher kinetic constants compared to the limited *in situ* observations from the ocean, particularly for K_m (i.e., culture-based K_m estimates of 9-544 μM ; Blackburne et al., 2007; Nowka et al., 2015; Ushiki et al., 2017).

Deleted: these

Deleted: K_m

483 The high K_m values derived for cultured NOB suggest that the affinity of these organisms for NO_2^- is
 484 low. However, this is not what is observed in the environment, which indicates that the most abundant
 485 marine NOB are not represented in the culture collection. For the Southern Ocean, we report high
 486 substrate affinities of NOB, with K_m values ranging from 134 to 403 nM, which is largely within the
 487 range documented for oxygenated coastal and open ocean waters (27-506 nM; Olson, 1981; Zhang et
 488 al., 2020) (Table 2). In the low- to zero-oxygen waters of the ETNP ODZ, similarly low K_m values have
 489 been reported (254 ± 161 nM; Sun et al., 2017), although values >5 μM have also been observed (Sun
 490 et al., 2021), with these latter estimates associated with ambient NO_2^- concentrations >1 μM . We explore
 491 the relationship between ambient NO_2^- concentration and K_m in detail in section 4.2 below. Our focus
 492 is on the K_m values derived under conditions of low ambient NO_2^- (i.e., <250 nM) given that (some of)
 493 the environmental factors affecting NO_2^- oxidation at high ambient NO_2^- concentrations appear to be
 494 unique. For example, oxygen has been shown to decrease the rate of NO_2^- oxidation in the ODZs (Sun
 495 et al., 2017, 2021) where novel clades of NOB have been detected (Sun et al., 2021). Additionally, NO_2^-
 496 concentrations in the oxygenated open ocean seldom exceed 250 nM (Zakem et al., 2018), in contrast
 497 to the ODZs (Bristow et al., 2016; Füssel et al., 2012).

Deleted: marine

Deleted: (27-506 nM; Zhang et al., 2020) and the and
oxygenated ...

Deleted: waters

Deleted: although

Deleted: have also been observed

Deleted: , with these

Deleted: (i.e., <250 nM)

Deleted: Additionally, NO_2^- concentrations in the
oxygenated open ocean seldom exceed 250 nM (Zakem et al.
2018), in contrast to the ODZs (Bristow et al., 2016; Füssel et
al., 2012).

498
 499
 500 Across our Southern Ocean transect, V_{\max} ranged from 5 to 14 nM d^{-1} , which is relatively low compared
 501 to estimates from other regions (Table 2), although such a comparison may not be particularly
 502 informative as our rates (and typically those of others) are not normalized for NOB abundance. Our
 503 V_{\max} estimates are also low compared to a previous study of mixed-layer nitrification in the winter
 504 Southern Ocean (Mdutyana et al., 2020). This difference may be partly due to the fact that the kinetics
 505 experiments were conducted using surface (~ 7 m) seawater (and thus, the surface NOB community that
 506 had been exposed to surface conditions, including elevated light), yet the highest rates of NO_2^- oxidation
 507 typically occur near the base of the mixed layer, including in the Southern Ocean (Figure 3b-e; Sun et
 508 al., 2017; Peng et al., 2018; Mdutyana et al., 2020). The opposite pattern has also been observed,
 509 however (although not in the Southern Ocean), with deeper samples yielding a lower V_{\max} than samples
 510 collected in shallow waters (Sun et al., 2017; Zhang et al., 2020).

Deleted: partly

Deleted: typically

Deleted: (although not in the Southern Ocean)

512 4.2 Environmental drivers of the NO_2^- oxidation kinetic parameters

513 We report maximum NO_2^- oxidation rates that generally increase towards the south and with decreasing
 514 SST (recognizing that these parameters co-vary), although St 01 in the STZ and St 06 and 07 in the
 515 MIZ deviate from this trend (Figure 4a and b; $R^2 = 0.019$; $p = 0.77$ and $R^2 = 0.12$; $p = 0.45$, respectively
 516 when all the stations are considered and $R^2 = 0.92$; $p = 0.041$ and $R^2 = 0.94$; $p = 0.029$, respectively,
 517 when St 01, 06, and 07 are excluded). It is possible that changes in the NOB community (composition
 518 and/or abundance) across the transect explains some of the observed variability. Nonetheless, taking
 519 latitude as a qualitative proxy for light, it is perhaps unsurprising that the maximum NO_2^- oxidation

535 rates increase southwards given that NOB are known to be at least partially light inhibited (Peng et al.,
 536 2018; Ward, 2005; Olson, 1981b). This [explanation](#) does not hold for the stations in the MIZ, however,
 537 at which V_{\max} decreases sharply despite these waters receiving the least light (less than 5 hours of weak
 538 sunlight, versus ~7 hours at 55°S to ~9 hours at 37°S). The temperature at the MIZ stations was <0°C,
 539 which raises the possibility of a temperature effect on V_{\max} . Indeed, we previously observed a strong
 540 decline in the V_{\max} associated with NH_4^+ oxidation at SSTs <0°C in the Southern Ocean, while at SSTs
 541 ranging from 0.6°C to 16°C, V_{\max} was near invariant (Mdutyana et al., 2022).

Deleted: explanation

542
 543 Marine nitrification has been reported to be largely unaffected by temperature variations (Bianchi et al.,
 544 1997; Horak et al., 2013; Baer et al., 2014), although NH_4^+ and NO_2^- oxidation may respond differently
 545 to similar changes in temperature. For example, marine NOB incubated at temperatures ranging from
 546 10°C to 35°C responded far more slowly to an increase in temperature than co-incubated AOA, resulting
 547 in an accumulation of NO_2^- in the incubation bottles (Schaefer and Hollibaugh 2017). By contrast, we
 548 previously observed no robust relationship between temperature and the maximum NH_4^+ oxidation rate
 549 in the Southern Ocean (Mdutyana et al., 2022), a finding that is consistent with studies of NH_4^+
 550 oxidation in the Arctic and temperate coastal ocean (Horak et al., 2013; Baer et al., 2014). Far less work
 551 has been done to assess the response of NOB to temperature changes. In the absence of experiments
 552 specifically designed to test the response of Southern Ocean NOB to temperature, it is difficult to
 553 disentangle the effect(s) on NO_2^- oxidation of temperature *versus* light (and possibly other parameters
 554 that co-vary with latitude, such as NO_2^- and/or micronutrient availability).

Deleted: (Mdutyana, 2021Mdutyana et al. 2022)

555
 556 Plotting V_{\max} as a function of the ambient substrate concentration ($[\text{NO}_2^-]_{\text{amb}}$) reveals a strong positive
 557 relationship for all but the MIZ stations (Figure 4c; $R^2 = 0.73$; $p = 0.065$ if the MIZ stations are
 558 excluded). In particular, the STZ station (St 01), which appeared anomalous in the plots of V_{\max} versus
 559 latitude and SST, is consistent with the other non-MIZ stations when evaluated in V_{\max} versus $[\text{NO}_2^-]_{\text{amb}}$
 560 space. The positive relationship of V_{\max} to $[\text{NO}_2^-]_{\text{amb}}$ could be taken as evidence that NO_2^- availability
 561 strongly controls the maximum achievable rate of NO_2^- oxidation. However, V_{\max} varies four-fold
 562 across the transect while $[\text{NO}_2^-]_{\text{amb}}$ only changes by a factor of two, and $[\text{NO}_2^-]_{\text{amb}}$ is also correlated with
 563 latitude ($R^2 = 0.51$, $p \leq 0.001$ for all surface $[\text{NO}_2^-]_{\text{amb}}$ data; Figure S2). Additionally, previous
 564 wintertime Southern Ocean NO_2^- oxidation rates (albeit not V_{\max}) showed no relationship with ambient
 565 NO_2^- concentration (Bianchi et al. 1997; Mdutyana et al. 2020). The extent to which V_{\max} is directly
 566 controlled by $[\text{NO}_2^-]_{\text{amb}}$ is thus unclear, and it is likely that NOB community composition, light
 567 availability, and temperature also play a role, with SST perhaps becoming more important at very low
 568 temperatures (i.e., in the MIZ).

Deleted: Mdutyana et al. 2022

Deleted: < 0.001

569
 570 Our estimates of K_m reveal that NOB in the wintertime Southern Ocean have a high affinity for NO_2^-
 571 that appears to decrease (i.e., the K_m rises) at higher latitudes (i.e., lower light) and lower temperatures,

576 with St 01 in the STZ again emerging as an exception (Figure 4d and e; $R^2 = 0.86$, $p = 0.008$ and $R^2 =$
 577 0.86 , $p = 0.008$, respectively). Plotting our K_m values as a function of $[\text{NO}_2^-]_{\text{amb}}$ reveals a strong positive
 578 relationship (Figure 4f; $R^2 = 0.83$, $p = 0.004$; black data points), implying that NO_2^- availability rather
 579 than temperature or light exerts the dominant control on K_m . This trend further suggests that NOB are
 580 well-adapted to the environment (or Southern Ocean region) in which they are found. Southern Ocean
 581 mixed-layer NO_2^- concentrations are almost never <150 nM, regardless of the season (Fripiat et al.
 582 2019; Mdutyana et al. 2020; Zakem et al. 2018), yet the relationship of K_m to $[\text{NO}_2^-]_{\text{amb}}$ also holds at far
 583 lower NO_2^- concentrations. The coloured data points in Figure 4f show K_m versus $[\text{NO}_2^-]_{\text{amb}}$ for four
 584 additional regions where a Michaelis-Menten relationship of NO_2^- oxidation rate to NO_2^- concentration
 585 was observed and where $[\text{NO}_2^-]_{\text{amb}}$ was <250 nM (two coastal ocean sites, the South China Sea (SCS;
 586 Zhang et al., 2020) and Southern California Bight (SCB; Olson, 1981); one oligotrophic ocean site, the
 587 subtropical South Atlantic (SSA; Fawcett et al. unpubl.); and two stations from the ETNP ODZ, where
 588 oxygen concentrations ranged from $0 \mu\text{M}$ to $16.8 \mu\text{M}$ (Sun et al., 2017)). The robust positive relationship
 589 of K_m to $[\text{NO}_2^-]_{\text{amb}}$ that emerges when these previous results are combined with our Southern Ocean
 590 data ($R^2 = 0.68$, $p < 0.001$) strongly implicates $[\text{NO}_2^-]_{\text{amb}}$ as the dominant control on the K_m of NO_2^-
 591 oxidation in the ocean, particularly at low $[\text{NO}_2^-]_{\text{amb}}$ (i.e., <250 nM).

Deleted: 008

Deleted: 008

Deleted: < 0.001

Deleted: (i.e., <250 nM).

592
 593
 594 The production of NO_2^- from NH_4^+ oxidation has recently been hypothesized to be vulnerable to iron
 595 limitation (Mdutyana et al., 2022) since AOB rely on iron-rich *cytochrome c* proteins (Arp et al., 2002;
 596 Walker et al., 2010) and some AOA appear to have a low affinity for inorganic iron (Shafiee et al.
 597 2019). NOB also contain iron-rich enzymes, such as nitrite oxidoreductase, which is responsible for
 598 converting NO_2^- to NO_3^- (Meincke et al., 1992; Spieck et al., 1998). While we have no iron data with
 599 which to compare our kinetic parameters, dissolved iron concentrations ($[\text{DFe}]$) were measured
 600 throughout the euphotic zone at the depth-profile stations (St 08 to St 11; Mdutyana et al., 2022). The
 601 revised NO_2^- oxidation rates at these stations are weakly positively correlated with $[\text{DFe}]$ ($R^2 = 0.35$, p
 602 $= 0.016$; Figure 5), indicating a potential role for iron in controlling NO_2^- oxidation. Combined with the
 603 evidence that iron may also constrain marine NH_4^+ oxidation (Shafiee et al., 2019), this observation
 604 implies that mixed-layer nitrification in the Southern Ocean may be iron-limited. Since phytoplankton
 605 consumption of regenerated NO_3^- yields no net removal of atmospheric CO_2 in a mass balance sense
 606 (Dugdale and Goering 1967; Yool et al., 2007), an iron-related control on mixed-layer nitrification
 607 would help to limit the extent to which this process can weaken the Southern Ocean's biological pump
 608 and would lead to enhanced competition between phytoplankton and nitrifiers for iron.

Deleted: Mdutyana et al. 2022

Deleted: throughout the euphotic zone

Deleted: Mdutyana et al., 2022

Deleted: in a mass balance sense (Dugdale and Goering 1967; Yool et al. 2007)

Deleted: and

Deleted: for iron

610 4.3 The persistence of elevated NO_2^- concentrations throughout the Southern Ocean's mixed layer

While still limited, there is growing evidence that marine AOA have a very high affinity for NH_4^+ (more correctly, ammonia (NH_3), the substrate for NH_4^+ oxidation; [Mdutyana et al., 2022](#); Martens-Habbena et al., 2009; Horak et al., 2013; Newell et al., 2013; Peng et al., 2016). Marine NOB also appear able to access low concentrations of substrate, based on the few *in situ* studies conducted to-date, including this one (Figure 4f; Olson, 1981; Sun et al., 2017; Zhang et al., 2020). This high substrate affinity is perhaps unsurprising given that NO_2^- concentrations are generally near-zero throughout the oxygenated ocean, rising modestly to values typically <500 nM at the PNM in (sub)tropical waters (Lomas and Lipschultz 2006; Zakem et al. 2018) and <400 nM over the mixed layer in (sub)polar regions (Zakem et al., 2018). The average surface NO_2^- concentration measured during Leg 1 of our cruise was 168 ± 48 nM (Figure 1a) and the average mixed-layer concentration for Leg 2 was 137 ± 57 nM (Figures 1b and 3a). Similar concentrations have been observed previously across the Southern Ocean, including in other seasons (Cavagna et al., 2015; Fripiat et al., 2019; Mdutyana et al., 2020). Thus, while NO_2^- oxidation in Southern Ocean surface waters is characterized by a low K_m , the affinity of NOB for NO_2^- is apparently not high enough to completely remove the available NO_2^- .

Deleted: Mdutyana et al. , 2022

The persistence of elevated NO_2^- concentrations in the mixed layer at high latitudes has [previously](#) been attributed to the inability of iron- and/or light-limited phytoplankton to fully consume NO_2^- transported to the surface with NO_3^- during deep mixing events (Zakem et al. 2018). However, subsurface NO_2^- concentrations in the Southern Ocean are typically below detection (Figure 1b and 3a; Olsen et al., 2016), so it is unclear how deep mixing could supply measurable NO_2^- to the euphotic zone. [We thus discount subsurface mixing as a primary explanation for the elevated Southern Ocean mixed-layer \$\text{NO}_2^-\$ concentrations, as were observed during our study and in other seasons \(e.g., Fripiat et al., 2019\).](#)

Deleted: previously

Deleted: . We thus discount subsurface mixing as a primary explanation for the elevated Southern Ocean mixed-layer NO_2^- concentrations, as were observed during our study and in other seasons (e.g., Fripiat et al. 2019). .

A second possible source of elevated mixed-layer NO_2^- is efflux following partial NO_3^- reduction to NO_2^- by phytoplankton (Lomas and Lipschultz 2006), which has been extensively documented in laboratory and field studies (see Collos, 1998 for a review). The release of NO_2^- by phytoplankton is hypothesized to result from light limitation of intracellular NO_2^- reduction (Vaccaro and Ryther 1960; Kiefer, Olson, and Holm-Hansen 1976), short-term increases in irradiance to which phytoplankton cannot adapt (Lomas and Lipschultz 2006), iron limitation of NO_3^- assimilation (Milligan and Harrison 2000), and/or release of phytoplankton from NO_3^- limitation following a period of starvation (Sciandra and Amara 1994). While some of these mechanisms may be ongoing in the Southern Ocean, they all require the initial uptake of NO_3^- by phytoplankton. This process occurs in the winter mixed layer at rates that are too low to support NO_2^- efflux to the extent that it would allow NO_2^- to accumulate to concentrations of 100 - ~~400~~ nM (Figure S3; Philibert et al., 2015; Mdutyana et al., 2020) while simultaneously being removed by NO_2^- oxidation. Additionally, we observe a reasonable correlation

Deleted: 400

665 between the NH_4^+ oxidation rates and the ambient NO_2^- concentration ($R^2 = 0.46$, $p < 0.001$; Figure S4),
 666 which implies that NO_2^- derives mainly from NH_4^+ oxidation rather than phytoplankton efflux.

667
 668 A third potential explanation for elevated mixed-layer NO_2^- is a decoupling of NH_4^+ and NO_2^- oxidation,
 669 which appears to be widespread in the environment (e.g., Ward and Zafiriou, 1988; Beman et al., 2013).
 670 In the oxygenated ocean, NH_4^+ oxidation has been considered the rate-limiting step in the nitrification
 671 pathway because NO_2^- seldom accumulates in the mixed layer (Kendall 1998; Kowalchuk and Stephen
 672 2001; Walker et al. 2010; Vajjala et al. 2013). However, rate measurements from numerous ocean
 673 regions show contrasting results, with NO_2^- oxidation sometimes outpacing NH_4^+ oxidation (Peng et al.
 674 2018; Dore and Karl 1996; Bristow et al. 2015; Horrigan et al. 1990) while in other cases, NH_4^+
 675 oxidation is dominant (Ward and Kilpatrick 1991; Kalvelage et al. 2013; Clark et al. 2008). The limited
 676 data available from previous Southern Ocean investigations show no clear trend (Bianchi et al., 1997;
 677 Mduyana et al., 2020). In the present study, mixed-layer corrNO_2^- rates are two- to seven-times lower
 678 than the coincidentally measured corrNH_4^+ (Figures 3 and 6). Additionally, the maximum rates of
 679 NO_2^- oxidation (V_{\max}) that we measure in this study for the surface NOB community (~5 to 13 nM d^{-1} ;
 680 Figure 2) are on average half those determined at the same stations for NH_4^+ oxidation (14 to 23 nM d^{-1} ;
 681 Mduyana et al., 2022). At the time of our sampling, therefore, NO_2^- oxidation was rate-limiting for
 682 nitrification, which likely accounts for much of the NO_2^- accumulated in the Southern Ocean's winter
 683 mixed layer .

684
 685 If a decoupling of NH_4^+ and NO_2^- oxidation is predominantly responsible for NO_2^- accumulation, an
 686 obvious question is why these rates are not balanced. Environmental factors like temperature and light
 687 may play a role (Ward, 2008), as may iron limitation and the different ecophysologies of NH_4^+ and
 688 NO_2^- oxidizers. AOA have been shown to adapt more rapidly than NOB to a change in temperature
 689 (Schaefer and Hollibaugh, 2017); however, seasonal SST changes within the various zones of the
 690 Southern Ocean are fairly small and the aforementioned study showing the differential thermal response
 691 of AOA and NOB was conducted at higher temperatures than those experienced in much of the Southern
 692 Ocean. With regards to light, there is evidence from culture and field studies that NOB are more
 693 photosensitive than AOA and AOB (Bock, 1965; Olson, 1981b; Qin et al., 2014). Our data are
 694 consistent with this notion insofar as the V_{\max} associated with NO_2^- oxidation in surface waters rises
 695 with increasing latitude (and thus decreasing light; Figure 4a) while the V_{\max} derived for NH_4^+ oxidation
 696 remains largely unchanged across >30 degrees of latitude (Mduyana et al., 2022). However, the
 697 ambient NO_2^- concentration in Southern Ocean surface waters rises near linearly with latitude (Figure
 698 S2a) while the NH_4^+ concentration resembles a step function, increasing from ~100 nM north of the
 699 SAF to ~700 nM south of the SAF, over a distance of roughly one degree of latitude (Figure S2b). The
 700 differing trends in V_{\max} may thus have more to do with substrate availability than photoinhibition.

701

Deleted: the

Deleted: concentration

Deleted: < 0

Deleted: 1

Deleted: that we measure in this study

Deleted: Mduyana et al. 2022

Deleted: much

Deleted: and

Deleted: changes

Deleted: Mduyana et al. 2022

Mixing, particularly deep winter overturning, might also contribute to a decoupling of NH_4^+ and NO_2^- oxidation. In coastal waters, deep winter mixing has been shown to dilute the nitrifier community, with AOO subsequently observed to recover more rapidly than NOB. This differential rate of recovery has been hypothesized to result in a period of low rates of NO_2^- oxidation during which the co-occurring NH_4^+ oxidation rates remain elevated, ultimately causing NO_2^- to accumulate in the surface layer (Haas et al., 2021). While a similar effect may play a role in NO_2^- accumulation in the open Southern Ocean, it is unlikely that the entire NO_2^- reservoir can be attributed to this process. The rates of NH_4^+ oxidation are only slightly higher than the NO_2^- oxidation rates in the winter mixed layer (Figure 3) and the mixed-layer NH_4^+ concentrations are elevated (Figure 3f). These observations imply that NH_4^+ oxidizers are limited by something other than NH_4^+ substrate,). These observations, them from catalysing higher rates of NO_2^- production (and thus NO_2^- accumulation).

Nitrite oxidoreductase (NXR), the enzyme possessed by NOB that is responsible for aerobic NO_2^- oxidation to NO_3^- , is an iron-sulfur molybdoprotein (Sundermeyer-Klinger et al. 1984; Meincke et al. 1992; Lucker et al. 2010). As such, NO_2^- oxidation has a significant iron requirement (Saito et al., 2020; Bayer et al., 2021), intimated by the relationship we observe between $\text{corrNO}_2^-_{\text{ox}}$ and DFe (Figure 5). Additionally, NO_2^- accumulation at the PNM in the California Current has been hypothesized to be caused by iron limitation of NOB (Santoro et al. 2013). AOB also require iron, in particular for the oxidation of hydroxylamine, which is catalyzed by the heme-rich hydroxylamine oxidoreductase complex (Arp et al., 2002; Walker et al., 2010). By contrast, AOA, the dominant marine NH_4^+ oxidizers, rely mainly on copper-containing proteins to mediate NH_4^+ oxidation (Amin et al., 2013; Walker et al., 2010; Santoro et al., 2015). In the iron-limited Southern Ocean, it is thus possible that iron scarcity more strongly limits NO_2^- than NH_4^+ oxidation. However, recent culture and proteomic work suggests that some AOA may actually have a high iron requirement (Alyson E. Santoro et al. 2015; Carini, Dupont, and Santoro 2018; Qin et al. 2018; Shafiee et al. 2019), and we have previously hypothesized an iron-related control on NH_4^+ oxidation in the Southern Ocean (Mdutyana et al., 2022). Deeper investigation is thus required to characterize the role of iron in controlling the relative rates of NH_4^+ and NO_2^- oxidation, and the implications for the complete nitrification pathway.

A further consideration is differences in the ecology of AOA and NOB. Marine NOB are an order of magnitude less abundant than AOA (e.g., Fussel et al., 2012; Beman et al., 2013b; Pachiadaki et al., 2017; Damashek et al., 2019; Kitzinger et al., 2020) and roughly three-times larger (Watson and Waterbury, 1971; Konneke et al., 2005; Martens-Habben et al., 2009; Pachiadaki et al., 2017). While marine NOB appear to have a high affinity for ambient NO_2^- , the *in situ* K_m values derived to-date are not as low as those reported for NH_4^+ oxidation (Horak et al., 2013; Peng et al., 2016; Xu et al., 2019; Zhang et al., 2020; Mdutyana et al. 2022), which is perhaps to be expected given the larger size of NOB versus AOA. Resource limitation theory posits that nitrifiers (NOB and AOA) require a

Deleted:

Deleted: with AOO subsequently observed to recover more rapidly than

Deleted: . This differential rate of recovery has been hypothesized to result in a period of,

Deleted: rates of

Deleted: during which the co-occurring

Deleted: to accumulate

Deleted: surface

Deleted: attributed

Deleted: the

Deleted: rates

Deleted:). These observations,

Deleted: which preventing prevents

Deleted: A number of studies have shown the negative effect of decreasing pH on NH_4^+ oxidation in the ocean (e.g., Huesemann et al., 2002; Beman et al., 2011; Kitidis et al., 2011), driven by a reduction in the proportion of NH_3 relative to NH_4^+ . By contrast, NO_2^- oxidation may increase as pH declines (Fulweiler et al., 2011; Heiss and Fulweiler, 2017), although such a correlation has only been observed in one coastal region. While a differential response of AOO and NOB to pH would decouple NH_4^+ and NO_2^- oxidation, the resultant trend should be one of higher NO_2^- accumulation in the northern Southern Ocean where surface pH is higher in winter and lower NO_2^- accumulation to the south where pH is lower (Key et al., 2004; McNeil and Matear, 2008) – this is not the meridional pattern that we observe (Figure 1b). ¶

Deleted: A. E.

Deleted: , Sayavedra-Soto, and Hommes

Deleted: Alyson E.

Deleted: Mdutyana et al. 2022

Deleted: marine NOB

Deleted: have a

Deleted: affinity for ambient NO_2^-

Deleted: Mdutyana et al. 2022

Deleted: size of NOB versus AOA.

Deleted: (NOB and AOA)

787 subsistence concentration of substrate (R^*) to maintain their population, and that those with the lowest
 788 R^* will outcompete all other organisms limited by the same resource, provided that their V_{\max} is higher
 789 than their loss rate due to grazing and/or viral lysis (Zakem et al., 2018). Because NOB are larger than
 790 AOA, they will have a higher R^* even before grazing pressure is factored in. Their larger size also
 791 means that NOB are more likely to be grazed than AOA, which will further increase their R^* , as will
 792 the fact that their maximum growth rates are low and thus vulnerable to being outpaced by their loss
 793 rate. Taken together, these factors will increase R^* , potentially resulting in the accumulation of NO_2^- in
 794 the water column, and may help to explain why the K_m for NO_2^- oxidation, in the Southern Ocean and
 795 elsewhere, is considerably higher than the K_m derived for NH_4^+ oxidation. Additionally, the fact that
 796 NOB will be preferentially grazed over AOA may contribute to NO_2^- oxidation being rate-limiting for
 797 nitrification.

798
 799 That NO_2^- oxidation was rate-limiting at the time of our sampling does not necessarily explain the
 800 accumulation of NO_2^- in the Southern Ocean mixed layer year-round. Neither NH_4^+ nor NO_2^- oxidation
 801 occur at elevated rates in summer or autumn (Bianchi et al., 1997; Mdotyana et al., 2020), yet the
 802 elevated NO_2^- concentrations persist during these seasons (Cavagna et al., 2015; Fripiat et al., 2019;
 803 Mdotyana et al., 2020). To fit a Michaelis-Menten function to our experimental data required amending
 804 the classical equation (equation 2) to allow for a positive x-intercept (i.e., a non-zero S value at which
 805 V was still zero, the C parameter in equation 3) (Archontoulis and Miguez, 2014). Additionally, at most
 806 stations, the NO_2^- oxidation rates did not increase substantially following the initial two or three
 807 substrate amendments (i.e., in Figure 2, the slope of the relationship between V and S is less steep for
 808 the initial two to three values of S than at higher S values). Practically, our findings suggest that
 809 Southern Ocean NOB require a minimum (i.e., “threshold”) NO_2^- concentration below which the NO_2^-
 810 concentration becomes severely limiting. Coupled with weak NO_2^- drawdown by iron- and/or light-
 811 limited phytoplankton during their incomplete consumption of the $\text{NO}_3^- + \text{NO}_2^-$ pool, a threshold
 812 substrate requirement of NOB can explain the year-round persistence of non-zero mixed-layer NO_2^-
 813 since it implies that there is no mechanism by which NO_2^- can be completely exhausted.

814
 815 The existence of a NO_2^- concentration threshold may indicate limitation of the membrane-bound NXR
 816 enzyme, either by NO_2^- or by another essential nutrient. Recently, using NXR concentrations, estimates
 817 of NXR specific activity, and direct measurements of *in situ* NO_2^- oxidation rates, Saito et al., (2020)
 818 deduced that *Nitrospina* NXR is undersaturated with NO_2^- in the tropical Pacific, possibly due to iron
 819 limitation. The authors suggest that under iron-scarce conditions, it becomes increasingly difficult for
 820 NOB to synthesize NXR and thus to oxidize NO_2^- . A similar dynamic may be at play in the Southern
 821 Ocean, with limited synthesis of NXR at low iron concentrations resulting in a decrease in the efficiency
 822 of the NO_2^- oxidation pathway that manifests most strongly when the ambient NO_2^- concentration is
 823 also low. This inefficiency could be alleviated at higher NO_2^- concentrations since NOB (even with a

Deleted: that

Deleted: higher

Deleted: the K_m

Deleted: function

Deleted: S

Deleted: the

Deleted: concentration

Deleted: The existence of a

Deleted: may indicate limitation of the membrane-bound

Deleted: enzyme, either by NO_2^- or by another essential nutrient. Recently, Using NXR concentrations, estimates of NXR specific activity, and direct measurements of *in situ* NO_2^- oxidation rates, Saito et al., (2020) recently deduced that *Nitrospina* NXR is undersaturated with NO_2^- in the iron-limited tropical Pacific, possibly due to iron limitation. The authors suggest that under iron-scarce conditions, it becomes increasingly difficult for NOB to synthesize NXR and thus to oxidize NO_2^- . A similar dynamic may be at play in the Southern Ocean, with limited synthesis of NXR at low iron concentrations resulting in a decrease in the efficiency of the NO_2^- oxidation pathway that manifests most strongly when the ambient NO_2^- concentration is also low. This inefficiency could be alleviated at higher NO_2^- concentrations since NOB (even with a paucity of NXR) are less likely to experience diffusion limitation with respect to NO_2^- when there is more of this substrate available (Pasciak and Gavis 1974). Regardless of its mechanistic basis, limitation of NOB NXR would help to explain the perennially high concentrations of NO_2^- in the Southern Ocean mixed layer. Moreover, environmental factors unique to the Southern Ocean, such as limited iron availability, may be instrumental in setting the NO_2^- threshold and associated elevated mixed-layer NO_2^- concentrations.¶

¶ Our observations raise the question of why a similar NO_2^- concentration threshold has not been reported for other ocean regions, particularly those characterized by similar conditions to the Southern Ocean. This may partly be due to the very limited number of NO_2^- oxidation kinetics experiments that have been conducted in the open ocean and/or to the fact that a classic Michaelis-Menten function is usually imposed upon kinetics data, with V assumed to increase as soon as $S > 0$. Additionally, depending on the maximum substrate concentration added during kinetics experiments (i.e., the maximum concentration on the x-axis of the V versus S plot), it can be difficult to discern a possible threshold NO_2^- concentration by simply examining the plots. Inspection of published Michaelis-Menten curves does reveal the possibility of a non-zero C value in some cases, including in the ETNP ODZ (Sun et al. 2021) and associated with the PNM in the South China Sea (Zhang et al. 2020). However, there are also published curves that clearly intercept the origin in V versus S space (Olson, 1981a; Sun et al., 2017), underscoring the need for further investigation of the conditions that lead to a threshold NO_2^- concentration requirement of NOB. , which is a membrane-bound enzyme that occurs in two forms: 1) with the substrate-binding subunit (NxrA) orientated outwards into the periplasmic space, as in *Nitrospira* and *Nitrospina* (Spieck et al., 1998; Lueker et al., 2010; 2013; Koeh et al., 2015; Daims et al., 2016) and 2) with NxrA orientated inward towards the cytoplasm, as in *Nitrococcus* and *Nitrobacter* (Spieck et al. ... [1]

paucity of NXR) are less likely to experience diffusion limitation with respect to NO_2^- when there is more of this substrate available (Pasciak and Gavis 1974). Regardless of its mechanistic basis, limitation of NOB NXR would help to explain the perennially high concentrations of NO_2^- in the Southern Ocean mixed layer. Moreover, environmental factors unique to the Southern Ocean, such as limited iron availability, may be instrumental in setting the NO_2^- threshold and associated elevated mixed-layer NO_2^- concentrations.

Our observations raise the question of why a similar NO_2^- concentration threshold has not been reported for other ocean regions, particularly those characterized by similar conditions to the Southern Ocean. This may partly be due to the very limited number of NO_2^- oxidation kinetics experiments that have been conducted in the open ocean and/or to the fact that a classic Michaelis-Menten function is usually imposed upon kinetics data, with V assumed to increase as soon as $S > 0$. Additionally, depending on the maximum substrate concentration added during kinetics experiments (i.e., the maximum concentration on the x-axis of the V versus S plot), it can be difficult to discern a possible threshold NO_2^- concentration by simply examining the plots. Inspection of published Michaelis-Menten curves does reveal the possibility of a non-zero C value in some cases, including in the ETNP ODZ (Sun et al., 2021) and associated with the PNM in the South China Sea (Zhang et al., 2020). However, there are also published curves that clearly intercept the origin in V versus S space (Olson, 1981a; Sun et al., 2017), underscoring the need for further investigation of the conditions that lead to a threshold NO_2^- concentration requirement of NOB.

5. Concluding remarks

In this study, we present the first NO_2^- oxidation kinetic constants for the Southern Ocean, derived from surface experiments conducted during winter 2017. All the experiments were well-described by the Michaelis-Menten equation, provided that a location parameter, C, was included in the model. V_{max} ranged from 5.2 ± 0.1 to $13 \pm 0.4 \text{ nM d}^{-1}$ and K_m ranged from 134 ± 8 to $403 \pm 24 \text{ nM}$, with the latter parameter showing a strong positive relationship with the ambient NO_2^- concentration. We interpret the positive values of C (range of 115 ± 2.3 to $245 \pm 18 \text{ nM}$) to indicate an ambient NO_2^- concentration threshold below which NOB, and thus NO_2^- oxidation, are impeded. We hypothesize that this threshold indicates substrate limitation of NXR, possibly exacerbated by the low ambient iron concentrations characteristic of the upper Southern Ocean. Our kinetics experiments were conducted in surface waters only, which raises the question of the relevance of our findings for deeper euphotic zone waters. For instance, it is possible that surface nitrifier communities may be more iron limited than those living nearer the base of the euphotic zone. However, in the winter Southern Ocean, the euphotic zone is always considerably shallower than the mixed layer (50-75 m versus 100-250 m) such that both layers are typically very well-mixed, as is apparent from the near-invariant mixed-layer (and thus euphotic-

Deleted: ¶

Nitrospina and *Nitrospira* are ubiquitous in the ocean (Beman et al., 2013; Füssel et al., 2012), which raises the question of why a similar NO_2^- concentration threshold has not been reported from other regions. This may partly be due to the very limited number of NO_2^- oxidation kinetics experiments that have been conducted in the open ocean and/or to the fact that a classic Michaelis-Menten function is usually imposed upon kinetics data, with V assumed to increase as soon as $S > 0$. Additionally, depending on the maximum substrate concentration added during kinetics experiments, it can be difficult to discern a possible threshold NO_2^- concentration by simply examining the resultant plots. Inspection of published Michaelis-Menten curves reveals the possibility of a non-zero C value in some cases, including in the ETNP ODZ (Sun et al., 2021) and associated with the PNM in the South China Sea (Zhang et al., 2020). However, there are other published curves that clearly do intercept the origin in V versus S space (Olson, 1981a; Sun et al., 2017), which may indicate a different NOB community (e.g., dominated by *Nitrococcus*). Alternately, environmental factors unique to the Southern Ocean, such as light, temperature, and/or iron availability, may be instrumental in setting the NO_2^- threshold and associated elevated mixed-layer NO_2^- concentrations that we observe. Indeed, iron limitation of NXR could be implicit in its tendency towards NO_2^- undersaturation. This finding is consistent with the mechanism we invoke to explain the apparent NO_2^- concentration threshold in the Southern Ocean, as well as with the existence of such a threshold indicating *Nitrospina* (and/or *Nitrospira*) dominance of the *in situ* NOB community. ¶

Deleted: ed

Deleted: , and thus NO_2^- oxidation, are

Deleted: W

Deleted: Our kinetics experiments were conducted in surface waters only, which raises the question of the relevance of our findings for deeper euphotic zone waters. For instance, it is possible that surface nitrifier communities may be more iron limited than those living nearer the base of the euphotic zone. However, in the winter Southern Ocean, the euphotic zone is always considerably shallower than the mixed layer (50-75 m versus 100-250 m) such that both layers are typically very well-mixed, as is apparent from the near-invariant mixed-layer (and thus euphotic-zone) distributions of nutrients (Fig 1b-c), including trace metals (Cloete et al. 2019). One might therefore expect the nitrifiers to also be evenly distributed over the euphotic zone and mixed layer. The light flux will not be homogenous over these layers, however. Indeed, light availability is frequently invoked to explain the vertical distribution of nitrification rates because nitrifier activity is impeded at high light. Our nitrification depth profiles do not show a vertical trend, instead remaining similar throughout the euphotic zone and only rising near the base of the mixed layer (Figure 3b-e). We thus consider the results of our surface kinetics experiments to be broadly applicable to the euphotic zone in winter.

zone) distributions of nutrients (Fig 1b-c), including trace metals (Cloete et al., 2019). One might therefore expect the nitrifiers to also be evenly distributed over the euphotic zone and mixed layer. The light flux will not be homogenous over these layers, however. Indeed, light availability is frequently invoked to explain the vertical distribution of nitrification rates because nitrifier activity is impeded at high light (Horrigan et al., 1981; Olson, 1981b; Qin et al., 2014; Peng et al., 2018). Our nitrification depth profiles do not show a vertical trend, instead remaining similar throughout the euphotic zone and only rising near the base of the mixed layer (Figure 3b-e). We thus consider the results of our surface kinetics experiments to be broadly applicable to the euphotic zone in winter. From the depth-profile measurements, we deduce that the rate-limiting step for mixed-layer nitrification in the winter Southern Ocean is NO_2^- oxidation. Despite this, NO_3^- production from NO_2^- oxidation accounted for 63-237% of the NO_3^- consumed by phytoplankton, consistent with previous wintertime observations from the Atlantic sector (Mdutyana et al., 2020). The implication of this finding is that most of the mixed-layer NO_3^- consumed by phytoplankton in winter, and likely also a significant fraction assimilated in spring, supports regenerated rather than new production (Yool et al., 2007; Mdutyana et al., 2020).

NO_2^- oxidation, as the ultimate pathway connecting reduced N to its most oxidized form (NO_3^-), is important throughout the water column, but particularly in the upper layer where the supply of reduced N is highest. The production of NO_3^- within the mixed layer from *in situ* nitrification can complicate the application of the new production paradigm as a framework for estimating carbon export potential, which advocates for additional measurements of this pathway over the upper ~200 m. Additionally, it is becoming increasingly clear that we lack a mechanistic understanding of the controls on nitrification (both NH_4^+ and NO_2^- oxidation), which renders it challenging to model both its magnitude and distribution, as well as to assess how these may change in future. In particular, further study of the role of iron in controlling nitrification is required, particularly in the Southern Ocean where the mixed layer's biological N cycle is dominated by nitrification in winter (Smart et al., 2015; Mdutyana et al., 2020) and surface-layer iron remains scarce throughout the year (Tagliabue et al., 2012).

Acknowledgements

We thank Captain Knowledge Bengu and the crew of the R/V *S.A. Agulhas II* and Chief Scientist M. Vichi for professional support during the cruise, as well as the Marine Biogeochemistry Lab team at the University of Cape Town (UCT), C. Karriem for extensive administrative support, and I. Newton and J. Luyt at the UCT Stable Light Isotope Laboratory for filter analyses. The nitrification measurements were made possible through the Princeton University Visiting Student Research Collaborator program- we are especially grateful to S. Oleynik in the Department of Geosciences for his expert assistance during the first author's visit. This work was supported by the South African National Research Foundation through Antarctic Programme grants to S.E.F. (110735, 129232), and S.J.T. (93076), and postgraduate scholarships to M.M. (112380), T.M. (114673 and 130826) and J.M.B. (110732); by UCT

Deleted: the

Deleted: Southern Ocean

Deleted: sector

Deleted: The implication of this finding is that

Deleted: pathway

Deleted: ing

Deleted: carbon

Deleted: potential

Deleted: remains scarce

Deleted: ¶

1101 through a Harry Crossley Foundation Research Fellowship to M.M., postgraduate scholarship to T.M.,
1102 Vice-Chancellor (VC) Research Scholarships to J.M.B., a VC Future Leaders 2030 award to S.E.F.,
1103 and a Research Committee Equipment grant to S.E.F.; by the African Academy of Sciences/Royal
1104 Society through a FLAIR Fellowship to S.E.F; and by US National Science Foundation grants to
1105 B.B.W. The authors also acknowledge the South African Department of Science and Innovation's
1106 Biogeochemistry Research Infrastructure Platform.

1107
1108
1109
1110

1111 **References**

- 1112 Amin, Shady A., James W. Moffett, Willm Martens-Habben, Jeremy E. Jacquot, Yang Han, Allan
1113 Devol, Anitra E. Ingalls, David A. Stahl, and E. Virginia Armbrust. 2013. "Copper
1114 Requirements of the Ammonia-Oxidizing Archaeon Nitrosopumilus Maritimus SCM1 and
1115 Implications for Nitrification in the Marine Environment." *Limnology and Oceanography* 58 (6):
1116 2037–45. <https://doi.org/10.4319/lo.2013.58.6.2037>.
- 1117 Archontoulis, Sotirios V., and Fernando E. Miguez. 2014. "Nonlinear Regression Models and
1118 Applications in Agricultural Research." *Agronomy Journal* 107 (2): 786–98.
1119 <https://doi.org/10.2134/agronj2012.0506>.
- 1120 Arp, Daniel J., Luis A. Sayavedra-Soto, and Norman G. Hommes. 2002. "Molecular Biology and
1121 Biochemistry of Ammonia Oxidation by Nitrosomonas Europaea." *Archives of Microbiology*
1122 178 (4): 250–55. <https://doi.org/10.1007/s00203-002-0452-0>.
- 1123 Baer, S. E., T. L. Connelly, R. E. Sipler, P. L. Yager, and D. A. Bronk. 2014. "Effect of Temperature
1124 on Rates of Ammonium Uptake and Nitrification in the Western Coastal Arctic during Winter,
1125 Spring, and Summer." *Global Biogeochemical Cycles* 28: 1455–66.
1126 <https://doi.org/10.1111/1462-2920.13280>.
- 1127 Bayer, Barbara, Mak A. Saito, Matthew R. McIlvin, Sebastian Lucker, Dawn M. Moran, Thomas S.
1128 Lankiewicz, Christopher L. Dupont, and Alyson E. Santoro. 2021. "Metabolic Versatility of the
1129 Nitrite-Oxidizing Bacterium Nitrospira Marina and Its Proteomic Response to Oxygen-Limited
1130 Conditions." *ISME Journal* 15 (4): 1025–39. <https://doi.org/10.1038/s41396-020-00828-3>.
- 1131 Belkin, Igor M., and Arnold L. Gordon. 1996. "Southern Ocean Fronts from the Greenwich Meridian
1132 to Tasmania." *Journal of Geophysical Research C: Oceans*. <https://doi.org/10.1029/95JC02750>.
- 1133 Beman, J. Michael, Joy Leilei Shih, and Brian N. Popp. 2013. "Nitrite Oxidation in the Upper Water
1134 Column and Oxygen Minimum Zone of the Eastern Tropical North Pacific Ocean." *ISME*
1135 *Journal* 7 (11): 2192–2205. <https://doi.org/10.1038/ismej.2013.96>.
- 1136 Beman, J. Michael, Brian N. Popp, and Christopher A. Francis. 2008. "Molecular and
1137 Biogeochemical Evidence for Ammonia Oxidation by Marine Crenarchaeota in the Gulf of
1138 California." *ISME Journal* 2 (4): 429–41. <https://doi.org/10.1038/ismej.2007.118>.
- 1139 Bianchi, Micheline, F. Feliatra, Paul Tréguer, Marie Anne Vincendeau, and Jean Morvan. 1997.
1140 "Nitrification Rates, Ammonium and Nitrate Distribution in Upper Layers of the Water Column
1141 and in Sediments of the Indian Sector of the Southern Ocean." *Deep-Sea Research Part II:*
1142 *Topical Studies in Oceanography* 44 (5): 1017–32. [https://doi.org/10.1016/S0967-](https://doi.org/10.1016/S0967-0645(96)00109-9)
1143 [0645\(96\)00109-9](https://doi.org/10.1016/S0967-0645(96)00109-9).
- 1144 Birch, Colin P.D. 1999. "A New Generalized Logistic Sigmoid Growth Equation Compared with the
1145 Richards Growth Equation." *Annals of Botany* 83 (6): 713–23.
1146 <https://doi.org/10.1006/anbo.1999.0877>.
- 1147 Blackburne, Richard, Vel M Vadivelu, and Zhiguo Yuan. 2007. "Kinetic Characterisation of an
1148 Enriched Nitrospira Culture with Comparison to Nitrobacter" 41: 3033–42.
1149 <https://doi.org/10.1016/j.watres.2007.01.043>.
- 1150 Bock, Eberhard. 1965. "Vergleichende Untersuchungen Über Die Wirkung Sichtbaren Lichtes Auf
1151 Nitrosomonas Europaea Und Nitrobacter Winogradskyi." *Archiv Für Mikrobiologie*.
1152 <https://doi.org/10.1007/BF00406848>.
- 1153 Bristow, Laura A., Tage Dalsgaard, Laura Tiano, Daniel B. Mills, Anthony D. Bertagnolli, Jody J.
1154 Wright, Steven J. Hallam, et al. 2016. "Ammonium and Nitrite Oxidation at Nanomolar Oxygen
1155 Concentrations in Oxygen Minimum Zone Waters." *Proceedings of the National Academy of*
1156 *Sciences* 113 (38): 10601–6. <https://doi.org/10.1073/pnas.1600359113>.

1157 Bristow, Laura A., Neha Sarode, John Cartee, Alejandro Caro-Quintero, Bo Thamdrup, and Frank J.
 1158 Stewart. 2015. "Biogeochemical and Metagenomic Analysis of Nitrite Accumulation in the Gulf
 1159 of Mexico Hypoxic Zone." *Limnology and Oceanography* 60 (5): 1733–50.
 1160 <https://doi.org/10.1002/lno.10130>.

1161 Caranto, Jonathan D., and Kyle M. Lancaster. 2017. "Nitric Oxide Is an Obligate Bacterial
 1162 Nitrification Intermediate Produced by Hydroxylamine Oxidoreductase." *Proceedings of the
 1163 National Academy of Sciences of the United States of America* 114 (31): 8217–22.
 1164 <https://doi.org/10.1073/pnas.1704504114>.

1165 Carini, Paul, Christopher L. Dupont, and Alyson E. Santoro. 2018. "Patterns of Thaumarchaeal Gene
 1166 Expression in Culture and Diverse Marine Environments." *Environmental Microbiology* 20 (6):
 1167 2112–24. <https://doi.org/10.1111/1462-2920.14107>.

1168 Carvalho, Filipa, Josh Kohut, Matthew J. Oliver, and Oscar Schofield. 2017. "Defining the
 1169 Ecologically Relevant Mixed-Layer Depth for Antarctica's Coastal Seas." *Geophysical
 1170 Research Letters*. <https://doi.org/10.1002/2016GL071205>.

1171 Cavagna, A. J., F. Fripiat, M. Elskens, P. Mangion, L. Chirurgien, I. Closset, M. Lasbleiz, et al. 2015.
 1172 "Production Regime and Associated N Cycling in the Vicinity of Kerguelen Island, Southern
 1173 Ocean." *Biogeosciences* 12 (21): 6515–28. <https://doi.org/10.5194/bg-12-6515-2015>.

1174 Clark, Darren R, Andrew P Rees, Ian Joint, Source Limnology, No Jan, Darren R Clark, Andrew P
 1175 Rees, and Ian Joint. 2008. "Ammonium Regeneration and Nitrification Rates in the Oligo
 1176 Trophic Atlantic Ocean : Implications for New Production Estimates." *Limnology and
 1177 Oceanography* 53 (1): 52–62.

1178 Cloete, R., J. C. Loock, T. Mtshali, S. Fietz, and A. N. Roychoudhury. 2019. "Winter and Summer
 1179 Distributions of Copper, Zinc and Nickel along the International GEOTRACES Section
 1180 GIPY05: Insights into Deep Winter Mixing." *Chemical Geology* 511 (February 2018): 342–57.
 1181 <https://doi.org/10.1016/j.chemgeo.2018.10.023>.

1182 Collos, Yves. 1998. "Nitrate Uptake, Nitrite Release and Uptake, and New Production Estimates."
 1183 *Marine Ecology Progress Series* 171: 293–301. <https://doi.org/10.3354/meps171293>.

1184 Damashek, Julian, Bradley B. Tolar, Qian Liu, Aimee O. Okotie-Oyekan, Natalie J. Wallsgrove,
 1185 Brian N. Popp, and James T. Hollibaugh. 2019. "Microbial Oxidation of Nitrogen Supplied as
 1186 Selected Organic Nitrogen Compounds in the South Atlantic Bight." *Limnology and
 1187 Oceanography* 64 (3): 982–95. <https://doi.org/10.1002/lno.11089>.

1188 DeVries, Tim, Mark Holzer, and Francois Primeau. 2017. "Recent Increase in Oceanic Carbon
 1189 Uptake Driven by Weaker Upper-Ocean Overturning." *Nature* 542 (7640): 215–18.
 1190 <https://doi.org/10.1038/nature21068>.

1191 Diaz, Frédéric, and Patrick Raimbault. 2000. "Nitrogen Regeneration and Dissolved Organic Nitrogen
 1192 Release during Spring in a NW Mediterranean Coastal Zone (Gulf of Lions): Implications for
 1193 the Estimation of New Production." *Marine Ecology Progress Series* 197: 51–65.
 1194 <https://doi.org/10.3354/meps197051>.

1195 DiFiore, Peter J., Daniel M. Sigman, and Robert B. Dunbar. 2009. "Upper Ocean Nitrogen Fluxes in
 1196 the Polar Antarctic Zone: Constraints from the Nitrogen and Oxygen Isotopes of Nitrate."
 1197 *Geochemistry, Geophysics, Geosystems* 10 (11). <https://doi.org/10.1029/2009GC002468>.

1198 Dore, John E, and David A I Karl. 1996. "Nitrification in the Euphotic Zone as a Source for Nitrite ,
 1199 Nitrate , and Nitrous Oxide at Station ALOHA" 41: 1619–28.

1200 Dugdale, R. C., and J. J. Goering. 1967. "Uptake of New and Regenerated Forms of Nitrogen in
 1201 Primary Productivity." *Limnology and Oceanography* 12 (2): 196–206.
 1202 <https://doi.org/10.4319/lo.1967.12.2.0196>.

1203 Dugdale, R C, and F P Wilkerson. 1986. "The Use of N-15 To Measure Nitrogen Uptake in Eutrophic
1204 Oceans - Experimental Considerations." *Limnology and Oceanography* 31 (4): 673–89.

1205 Eppley, Richard W., and Bruce J. Peterson. 1979. "Particulate Organic Matter Flux and Planktonic
1206 New Production in the Deep Ocean." *Nature* 282 (5740): 677–80.
1207 <https://doi.org/10.1038/282677a0>.

1208 Fripiat, François, Anja S. Studer, Gerald H. Haug, Sergey Oleynik, Alfredo Martínez-García, Sandi
1209 M. Smart, Florian Rubach, Daniel M. Sigman, Sarah E. Fawcett, and Preston C. Kemeny. 2019.
1210 "The Isotope Effect of Nitrate Assimilation in the Antarctic Zone: Improved Estimates and
1211 Paleoceanographic Implications." *Geochimica et Cosmochimica Acta* 247: 261–79.
1212 <https://doi.org/10.1016/j.gca.2018.12.003>.

1213 Füssel, Jessika, Phyllis Lam, Gaute Lavik, Marlene M. Jensen, Moritz Holtappels, Marcel Günter, and
1214 Marcel M.M. Kuypers. 2012. "Nitrite Oxidation in the Namibian Oxygen Minimum Zone."
1215 *ISME Journal* 6 (6): 1200–1209. <https://doi.org/10.1038/ismej.2011.178>.

1216 Glibert, Patricia M., Mark R. Dennett, and Joel C. Goldman. 1985. "Inorganic Carbon Uptake by
1217 Phytoplankton in Vineyard Sound, Massachusetts. II. Comparative Primary Productivity and
1218 Nutritional Status of Winter and Summer Assemblages." *Journal of Experimental Marine
1219 Biology and Ecology* 86 (2). [https://doi.org/10.1016/0022-0981\(85\)90025-5](https://doi.org/10.1016/0022-0981(85)90025-5).

1220 Glibert, Patricia M., Fredric Lipschultz, James J. McCarthy, and Mark A. Altabet. 1982. "Isotope
1221 Dilution Models of Uptake and Remineralization of Ammonium By Marine Plankton."
1222 *Limnology and Oceanography* 27 (4): 639–50. <https://doi.org/10.4319/lo.1982.27.4.0639>.

1223 Grasshoff K, Ehrhardt M, and Kremling K. 1983. *Methods of Seawater Analysis*. Verlag Chemie,
1224 New York.

1225 Gruber, Nicolas, Dominic Clement, Brendan R. Carter, Richard A. Feely, Steven van Heuven, Mario
1226 Hoppema, Masao Ishii, et al. 2019. "The Oceanic Sink for Anthropogenic CO₂ from 1994 to
1227 2007." *Science* 363 (6432): 1193–99. <https://doi.org/10.1126/science.aau5153>.

1228 Haas, Sebastian, Brent M. Robicheau, Subhadeep Rakshit, Jennifer Tolman, Christopher K. Algar,
1229 Julie LaRoche, and Douglas W.R. Wallace. 2021. "Physical Mixing in Coastal Waters Controls
1230 and Decouples Nitrification via Biomass Dilution." *Proceedings of the National Academy of
1231 Sciences of the United States of America* 118 (18). <https://doi.org/10.1073/pnas.2004877118>.

1232 Hauck, J., C. Völker, D. A. Wolf-Gladrow, C. Laufkötter, M. Vogt, O. Aumont, L. Bopp, et al. 2015.
1233 "On the Southern Ocean CO₂ Uptake and the Role of the Biological Carbon Pump in the 21st
1234 Century." *Global Biogeochemical Cycles* 29 (9): 1451–70.
1235 <https://doi.org/10.1002/2015GB005140>.

1236 Heiss, Elise M., and Robinson W. Fulweiler. 2017. "Erratum to 'Coastal Water Column Ammonium
1237 and Nitrite Oxidation Are Decoupled in Summer' (Estuarine, Coastal and Shelf Science (2016)
1238 178 (110–119) (S0272771417301981) (10.1016/j.ecss.2017.02.023))." *Estuarine, Coastal and
1239 Shelf Science* 193: 37–45. <https://doi.org/10.1016/j.ecss.2016.12.026>.

1240 Holmes, R M, A Aminot, R Kerouel, B A Hooker, and B J Peterson. 1999. "A Simple and Precise
1241 Method for Measuring Ammonium in Marine and Freshwater Ecosystems." *Canadian Journal
1242 of Fisheries and Aquatic Sciences*. <https://doi.org/10.1139/cjfas-56-10-1801>.

1243 Horak, Rachel E.A., Wei Qin, Andy J. Schauer, E. Virginia Armbrust, Anitra E. Ingalls, James W.
1244 Moffett, David A. Stahl, and Allan H. Devol. 2013. "Ammonia Oxidation Kinetics and
1245 Temperature Sensitivity of a Natural Marine Community Dominated by Archaea." *ISME
1246 Journal* 7 (10): 2023–33. <https://doi.org/10.1038/ismej.2013.75>.

1247 Horrigan, S. G., J. P. Montoya, J. L. Nevins, J. J. McCarthy, H. Ducklow, R. Goericke, and T.
1248 Malone. 1990. "Nitrogenous Nutrient Transformations in the Spring and Fall in the Chesapeake

1249 Bay." *Estuarine, Coastal and Shelf Science* 30 (4). [https://doi.org/10.1016/0272-7714\(90\)90004-](https://doi.org/10.1016/0272-7714(90)90004-B)
1250 B.

1251 Jacob, Juliane, Boris Nowka, Véronique Merten, Tina Sanders, Eva Spieck, and Kirstin Dähnke.
1252 2017. "Oxidation Kinetics and Inverse Isotope Effect of Marine Nitrite-Oxidizing Isolates."
1253 *Aquatic Microbial Ecology* 80 (3): 289–300. <https://doi.org/10.3354/ame01859>.

1254 Jong, Ehlke de, Marcello Vichi, Carolin Birgitta Mehlmann, Clare Eayrs, Wade De Kock, Marcel
1255 Moldenhauer, and Riesna Reuben Audh. 2018. "Sea Ice Conditions within the Antarctic
1256 Marginal Ice Zone in Winter 2017, Onboard the SA Agulhas II." *Pangaea*, 2018.
1257 <https://doi.org/10.1594/PANGAEA.885211>.

1258 Kalvelage, Tim, Gaute Lavik, Phyllis Lam, Sergio Contreras, Lionel Arteaga, Carolin R. Löscher,
1259 Andreas Oeschlies, Aurélien Paulmier, Lothar Stramma, and Marcel M.M. Kuypers. 2013.
1260 "Nitrogen Cycling Driven by Organic Matter Export in the South Pacific Oxygen Minimum
1261 Zone." *Nature Geoscience* 6 (3): 228–34. <https://doi.org/10.1038/ngeo1739>.

1262 Kendall, Carol. 1998. "USGS -- Isotope Tracers -- Resources: Isotope Tracers in Catchment
1263 Hydrology -- Chapter 16." *Isotope Tracers in Catchment Hydrology Elsevier Science B.V.*

1264 Khatiwala, S., F. Primeau, and T. Hall. 2009. "Reconstruction of the History of Anthropogenic CO2
1265 Concentrations in the Ocean." *Nature* 462 (7271): 346–49. <https://doi.org/10.1038/nature08526>.

1266 Kiefer, D. A., R. J. Olson, and O. Holm-Hansen. 1976. "Another Look at the Nitrite and Chlorophyll
1267 Maxima in the Central North Pacific." *Deep-Sea Research and Oceanographic Abstracts* 23
1268 (12). [https://doi.org/10.1016/0011-7471\(76\)90895-0](https://doi.org/10.1016/0011-7471(76)90895-0).

1269 Kits, K. Dimitri, Christopher J. Sedlacek, Elena V. Lebedeva, Ping Han, Alexandr Bulaev, Petra
1270 Pjevac, Anne Daebeler, et al. 2017. "Kinetic Analysis of a Complete Nitrifier Reveals an
1271 Oligotrophic Lifestyle." *Nature* 549 (7671): 269–72. <https://doi.org/10.1038/nature23679>.

1272 Kitzinger, Katharina, Hannah K. Marchant, Laura A. Bristow, Craig W. Herbold, Cory C. Padilla,
1273 Abiel T. Kidane, Sten Littmann, et al. 2020. "Single Cell Analyses Reveal Contrasting Life
1274 Strategies of the Two Main Nitrifiers in the Ocean." *Nature Communications* 11 (1).
1275 <https://doi.org/10.1038/s41467-020-14542-3>.

1276 Kowalchuk, G. A., and J. R. Stephen. 2001. "Ammonia-Oxidizing Bacteria: A Model for Molecular
1277 Microbial Ecology." *Annual Review of Microbiology* 55: 485–529.
1278 <https://doi.org/10.1146/annurev.micro.55.1.485>.

1279 Kozłowski, Jessica A., Michaela Stieglmeier, Christa Schleper, Martin G. Klotz, and Lisa Y. Stein.
1280 2016. "Pathways and Key Intermediates Required for Obligate Aerobic Ammonia-Dependent
1281 Chemolithotrophy in Bacteria and Thaumarchaeota." *ISME Journal* 10 (8): 1836–45.
1282 <https://doi.org/10.1038/ismej.2016.2>.

1283 Lomas, Michael W., and Fredric Lipschultz. 2006. "Forming the Primary Nitrite Maximum: Nitrifiers
1284 or Phytoplankton?" *Limnology and Oceanography* 51 (5): 2453–67.
1285 <https://doi.org/10.4319/lo.2006.51.5.2453>.

1286 Lückner, Sebastian, Michael Wagner, Frank Maixner, Eric Pelletier, Hanna Koch, Benoit Vacherie,
1287 Thomas Rattei, et al. 2010. "A Nitrospira Metagenome Illuminates the Physiology and
1288 Evolution of Globally Important Nitrite-Oxidizing Bacteria." *Proceedings of the National
1289 Academy of Sciences of the United States of America* 107 (30): 13479–84.
1290 <https://doi.org/10.1073/pnas.1003860107>.

1291 Martens-Habbena, Willm, Paul M. Berube, Hidetoshi Urakawa, José R. De La Torre, and David A.
1292 Stahl. 2009. "Ammonia Oxidation Kinetics Determine Niche Separation of Nitrifying Archaea
1293 and Bacteria." *Nature* 461 (7266): 976–79. <https://doi.org/10.1038/nature08465>.

1294 McIlvin, Matthew R., and Karen L. Casciotti. 2011. "Technical Updates to the Bacterial Method for

1295 Nitrate Isotopic Analyses.” *Analytical Chemistry* 83 (5): 1850–56.
1296 <https://doi.org/10.1021/ac1028984>.

1297 Mdutyana, Mhlangabezi. 2021. “Mixed Layer Nitrogen Cycling in the Southern Ocean: Seasonality,
1298 Kinetics, and Biogeochemical Implications A Thesis Presented for the Degree Of.” *University of*
1299 *Cape Town, PhD Thesis*, no. June.

1300 Mdutyana, Mhlangabezi, Xin Sun, Jessica Burger, Raquel Flynn, Shantelle Smith, Natasha R. van
1301 Horsten, Eva Bucciarelli, et al. 2022. “The Kinetics of Ammonium Uptake and Oxidation during
1302 Winter across the Indian Sector of the Southern Ocean.” *Limnology and Oceanography*, 1–19.
1303 <https://doi.org/10.1002/lno.12050>.

1304 Mdutyana, Mhlangabezi, Sandy J. Thomalla, R. Philibert, Bess B. Ward, and Sarah E. Fawcett. 2020.
1305 “The Seasonal Cycle of Nitrogen Uptake and Nitrification in the Atlantic Sector of the Southern
1306 Ocean.” *Global Biogeochemical Cycles*, no. 3: 1–29. <https://doi.org/10.1029/2019GB006363>.

1307 Meincke, Michael, Eberhard Bock, Dieter Kastrau, and Peter M.H. Kroneck. 1992. “Nitrite
1308 Oxidoreductase from *Nitrobacter Hamburgensis*: Redox Centers and Their Catalytic Role.”
1309 *Archives of Microbiology* 158 (2): 127–31. <https://doi.org/10.1007/BF00245215>.

1310 Milligan, Allen J., and Paul J. Harrison. 2000. “Effects of Non-Steady-State Iron Limitation on
1311 Nitrogen Assimilatory Enzymes in the Marine Diatom *Thalassiosira weissflogii*
1312 (*Bacillariophyceae*).” *Journal of Phycology* 36 (1): 78–86. [https://doi.org/10.1046/j.1529-](https://doi.org/10.1046/j.1529-8817.2000.99013.x)
1313 [8817.2000.99013.x](https://doi.org/10.1046/j.1529-8817.2000.99013.x).

1314 Monod, Jacques. 1942. “Recherches Sur La Croissance Des Cultures Bacteriennes.” *Hermann and*
1315 *Cie, Paris*.

1316 Mulholland, Margaret R., and Peter W. Bernhardt. 2005. “The Effect of Growth Rate, Phosphorus
1317 Concentration, and Temperature on N₂ Fixation, Carbon Fixation, and Nitrogen Release in
1318 Continuous Cultures of *Trichodesmium* IMS101.” *Limnology and Oceanography* 50 (3): 839–
1319 49. <https://doi.org/10.4319/lo.2005.50.3.0839>.

1320 Newell, Silvia E., Andrew R. Babbín, Amal Jayakumar, and Bess B. Ward. 2011. “Ammonia
1321 Oxidation Rates and Nitrification in the Arabian Sea.” *Global Biogeochemical Cycles* 25 (4): 1–
1322 10. <https://doi.org/10.1029/2010GB003940>.

1323 Newell, Silvia E., Sarah E. Fawcett, and Bess B. Ward. 2013. “Depth Distribution of Ammonia
1324 Oxidation Rates and Ammonia-Oxidizer Community Composition in the Sargasso Sea.”
1325 *Limnology and Oceanography* 58 (4): 1491–1500. <https://doi.org/10.4319/lo.2013.58.4.1491>.

1326 Nowka, Boris, Holger Daims, and Eva Spieck. 2015. “Comparison of Oxidation Kinetics of Nitrite-
1327 Oxidizing Bacteria : Nitrite Availability as a Key Factor in Niche Differentiation” 81 (2): 745–
1328 53. <https://doi.org/10.1128/AEM.02734-14>.

1329 Olsen, Are, Alex Kozyr, Siv K. Lauvset, Mario Hoppema, Fiz F. Pérez, Reiner Steinfeldt, Sara
1330 Jutterström, et al. 2016. “The Global Ocean Data Analysis Project Version 2 (GLODAPv2) – an
1331 Internally Consistent Data Product for the World Ocean.” *Earth System Science Data* 8 (2):
1332 297–323. <https://doi.org/10.5194/essd-8-297-2016>.

1333 Olson, R.J. 1981a. “¹⁵N Tracer Studies of the Primary Nitrite Maximum.” *Journal of Marine*
1334 *Research* 39 (Number 2): 203–26.

1335 ———. 1981b. “Differential Photoinhibition of Marine Nitrifying Bacteria - a Possible Mechanism
1336 for the Formation of the Primary Nitrite Maximum.” *Journal of Marine Research* 39 (2): 227–
1337 38.

1338 Orsi, H, Thomas Whitworth, and Worth D Nowlin Jr. 1995. “On the Meridional Extent and Fronts of
1339 the Antarctic Circumpolar Current Pronounced Meridional Gradients in Surface Properties
1340 Separate Waters of the Southern Ocean from the Warmer and Saltier Waters of the Subtropical

1341 Circulations.” *Deep Sea Research* 42 (5): 641–73. [https://doi.org/10.1016/0967-0637\(95\)00021-](https://doi.org/10.1016/0967-0637(95)00021-)
1342 W.

1343 Pachiadaki, Maria G, Eva Sintes, Kristin Bergauer, Julia M Brown, Nicholas R Record, Brandon K
1344 Swan, and Mary Elizabeth Mathyer. 2017. “Major Role of Nitrite-Oxidizing Bacteria in Dark
1345 Ocean Carbon Fixation” 1051 (November): 1046–51.

1346 Pasciak, Walter J, and Jerome Gavis. 1974. “Transport Limitation of Nutrient Uptake in
1347 Phytoplankton.” *Limnology and Oceanography* 19 (6): 881–88.

1348 Peng, Xuefeng, Sarah E. Fawcett, Nicolas van Oostende, Martin J. Wolf, Dario Marconi, Daniel M.
1349 Sigman, and Bess B. Ward. 2018. “Nitrogen Uptake and Nitrification in the Subarctic North
1350 Atlantic Ocean.” *Limnology and Oceanography*, no. 1967. <https://doi.org/10.1002/lno.10784>.

1351 Peng, Xuefeng, Clara A. Fuchsman, Amal Jayakumar, Sergey Oleynik, Willm Martens-Habbena,
1352 Allan H. Devol, and Bess B. Ward. 2015. “Ammonia and Nitrite Oxidation in the Eastern
1353 Tropical North Pacific.” *Global Biogeochemical Cycles* 29 (12): 2034–49.
1354 <https://doi.org/10.1002/2015GB005278>.

1355 Peng, Xuefeng, Clara A. Fuchsman, Amal Jayakumar, Mark J. Warner, Allan H. Devol, and Bess B.
1356 Ward. 2016. “Revisiting Nitrification in the Eastern Tropical South Pacific: A Focus on
1357 Controls.” *Journal of Geophysical Research: Oceans*. <https://doi.org/10.1002/2015JC011455>.

1358 Philibert, R., H. Waldron, and D. Clark. 2015. “A Geographical and Seasonal Comparison of
1359 Nitrogen Uptake by Phytoplankton in the Southern Ocean.” *Ocean Science* 11 (2): 251–67.
1360 <https://doi.org/10.5194/os-11-251-2015>.

1361 Pollard, R. T., M. I. Lucas, and J. F. Read. 2002. “Physical Controls on Biogeochemical Zonation in
1362 the Southern Ocean.” *Deep-Sea Research Part II: Topical Studies in Oceanography* 49 (16):
1363 3289–3305. [https://doi.org/10.1016/S0967-0645\(02\)00084-X](https://doi.org/10.1016/S0967-0645(02)00084-X).

1364 Qin, Wei, Shady A. Amin, Rachel A. Lundeen, Katherine R. Heal, Willm Martens-Habbena, Serdar
1365 Turkarslan, Hidetoshi Urakawa, et al. 2018. “Stress Response of a Marine Ammonia-Oxidizing
1366 Archaeon Informs Physiological Status of Environmental Populations.” *ISME Journal* 12 (2):
1367 508–19. <https://doi.org/10.1038/ismej.2017.186>.

1368 Qin, Wei, Shady A. Amin, Willm Martens-Habbena, Christopher B. Walker, Hidetoshi Urakawa,
1369 Allan H. Devol, Anitra E. Ingalls, James W. Moffett, E. Virginia Armbrust, and David A. Stahl.
1370 2014. “Marine Ammonia-Oxidizing Archaeal Isolates Display Obligate Mixotrophy and Wide
1371 Ecotypic Variation.” *Proceedings of the National Academy of Sciences of the United States of*
1372 *America* 111 (34): 12504–9. <https://doi.org/10.1073/pnas.1324115111>.

1373 Raven, J. A., and P. G. Falkowski. 1999. “Oceanic Sinks for Atmospheric CO₂.” *Plant, Cell and*
1374 *Environment* 22 (6): 741–55. <https://doi.org/10.1046/j.1365-3040.1999.00419.x>.

1375 Read, J. F., R. T. Pollard, and U. Bathmann. 2002. “Physical and Biological Patchiness of an Upper
1376 Ocean Transect from South Africa to the Ice Edge near the Greenwich Meridian.” *Deep-Sea*
1377 *Research Part II: Topical Studies in Oceanography* 49 (18): 3713–33.
1378 [https://doi.org/10.1016/S0967-0645\(02\)00108-X](https://doi.org/10.1016/S0967-0645(02)00108-X).

1379 Rees, Andrew P., Ian Joint, and Kirsten M. Donald. 1999. “Early Spring Bloom Phytoplankton-
1380 Nutrient Dynamics at the Celtic Sea Shelf Edge.” *Deep-Sea Research Part I: Oceanographic*
1381 *Research Papers*. [https://doi.org/10.1016/S0967-0637\(98\)00073-9](https://doi.org/10.1016/S0967-0637(98)00073-9).

1382 Saito, Mak A., Matthew R. McIlvin, Dawn M. Moran, Alyson E. Santoro, Chris L. Dupont, Patrick A.
1383 Rafter, Jaclyn K. Saunders, et al. 2020. “Abundant Nitrite-Oxidizing Metalloenzymes in the
1384 Mesopelagic Zone of the Tropical Pacific Ocean.” *Nature Geoscience* 13 (5): 355–62.
1385 <https://doi.org/10.1038/s41561-020-0565-6>.

1386 Santoro, A. E., C. M. Sakamoto, J. M. Smith, J. N. Plant, A. L. Gehman, A. Z. Worden, K. S.

1387 Johnson, C. A. Francis, and K. L. Casciotti. 2013. "Measurements of Nitrite Production in and
1388 around the Primary Nitrite Maximum in the Central California Current." *Biogeosciences* 10
1389 (11): 7395–7410. <https://doi.org/10.5194/bg-10-7395-2013>.

1390 Santoro, Alyson E., Christopher L. Dupont, R. Alex Richter, Matthew T. Craig, Paul Carini, Matthew
1391 R. McIlvin, Youngik Yang, William D. Orsi, Dawn M. Moran, and Mak A. Saito. 2015.
1392 "Genomic and Proteomic Characterization of 'Candidatus Nitrosopelagicus Brevis': An
1393 Ammonia-Oxidizing Archaeon from the Open Ocean." *Proceedings of the National Academy of
1394 Sciences of the United States of America* 112 (4): 1173–78.
1395 <https://doi.org/10.1073/pnas.1416223112>.

1396 Schaefer, Sylvia C., and James T. Hollibaugh. 2017. "Temperature Decouples Ammonium and Nitrite
1397 Oxidation in Coastal Waters." *Environmental Science and Technology* 51 (6): 3157–64.
1398 <https://doi.org/10.1021/acs.est.6b03483>.

1399 Schofield, Oscar, Travis Miles, Anne Carlijn Alderkamp, Sang Hoon Lee, Christina Haskins, Emily
1400 Rogalsky, Rachel Sipler, Robert M. Sherrell, and Patricia L. Yager. 2015. "In Situ
1401 Phytoplankton Distributions in the Amundsen Sea Polynya Measured by Autonomous Gliders."
1402 *Elementa*. <https://doi.org/10.12952/journal.elementa.000073>.

1403 Sciandra, A., and R. Amara. 1994. "Effects of Nitrogen Limitation on Growth and Nitrite Excretion
1404 Rates of the Dinoflagellate *Prorocentrum Minimum*." *Marine Ecology Progress Series* 105 (3):
1405 301. <https://doi.org/10.3354/meps105301>.

1406 Shafiee, Roxana T., Joseph T. Snow, Qiong Zhang, and Rosalind E. M. Rickaby. 2019. "Iron
1407 Requirements and Uptake Strategies of the Globally Abundant Marine Ammonia-Oxidising
1408 Archaeon, *Nitrosopumilus Maritimus* SCM1." *The ISME Journal*.
1409 <https://doi.org/10.1038/s41396-019-0434-8>.

1410 Sigman, D. M., K. L. Casciotti, M. Andreani, C. Barford, M. Galanter, and J. K. Böhlke. 2001. "A
1411 Bacterial Method for the Nitrogen Isotopic Analysis of Nitrate in Seawater and Freshwater."
1412 *Analytical Chemistry* 73 (17): 4145–53. <https://doi.org/10.1021/ac010088e>.

1413 Smart, Sandi M, Sarah E Fawcett, Sandy J Thomalla, Mira a Weigand, Chris J C Reason, and Daniel
1414 M Sigman. 2015. "Global Biogeochemical Cycles," 1–19.
1415 <https://doi.org/10.1002/2014GB005013>.Received.

1416 Smith, Shantelle, Katye E. Altieri, Mhlangabezi Mduyana, David R. Walker, Ruan G. Parrott, Sedick
1417 Gallie, Kurt A.M. Spence, Jessica M. Burger, and Sarah E. Fawcett. 2022. "Biogeochemical
1418 Controls on Ammonium Accumulation in the Surface Layer of the Southern Ocean."
1419 *Biogeosciences* 19 (3): 715–41. <https://doi.org/10.5194/bg-19-715-2022>.

1420 Sorokin, Dmitry Y., Sebastian Lucker, Dana Vejmelkova, Nadezhda A. Kostrikina, Robbert
1421 Kleerebezem, W. Irene C. Rijpstra, Jaap S. Sinninghe Damsté, et al. 2012. "Nitrification
1422 Expanded: Discovery, Physiology and Genomics of a Nitrite-Oxidizing Bacterium from the
1423 Phylum Chloroflexi." *ISME Journal* 6 (12): 2245–56. <https://doi.org/10.1038/ismej.2012.70>.

1424 Spieck, Eva, Silke Ehrich, and Jens Aamand. 1998. "Isolation and Immunocytochemical Location of
1425 the Nitrite-Oxidizing System in *Nitrospira Moscoviensis*." *Arch Microbiol*, no. 169: 225–30.

1426 Sun, Xin, Claudia Frey, Emilio Garcia-Robledo, Amal Jayakumar, and Bess B. Ward. 2021.
1427 "Microbial Niche Differentiation Explains Nitrite Oxidation in Marine Oxygen Minimum
1428 Zones." *The ISME Journal*, 1–13. <https://doi.org/10.1038/s41396-020-00852-3>.

1429 Sun, Xin, Qixing Ji, Amal Jayakumar, and Bess B. Ward. 2017. "Dependence of Nitrite Oxidation on
1430 Nitrite and Oxygen in Low-Oxygen Seawater." *Geophysical Research Letters* 44 (15): 7883–91.
1431 <https://doi.org/10.1002/2017GL074355>.

1432 Sundermeyer-Klinger, Hilke, Wolfgang Meyer, Beate Warninghoff, and Eberhard Bock. 1984.

1433 “Membrane-Bound Nitrite Oxidoreductase of Nitrobacter: Evidence for a Nitrate Reductase
1434 System.” *Archives of Microbiology* 140 (2–3). <https://doi.org/10.1007/BF00454918>.

1435 Tagliabue, A., T. Mtshali, O. Aumont, A. R. Bowie, M. B. Klunder, A. N. Roychoudhury, and S.
1436 Swart. 2012. “A Global Compilation of Dissolved Iron Measurements: Focus on Distributions
1437 and Processes in the Southern Ocean.” *Biogeosciences* 9 (6): 2333–49.
1438 <https://doi.org/10.5194/bg-9-2333-2012>.

1439 Tsoularis, A., and J. Wallace. 2002. “Analysis of Logistic Growth Models.” *Mathematical Biosciences*
1440 179: 21–55.

1441 Ushiki, Norisuke, Masaru Jinno, Hirotosugu Fujitani, Toshikazu Suenaga, Akihiko Terada, and Satoshi
1442 Tsuneda. 2017. “Nitrite Oxidation Kinetics of Two Nitrospira Strains : The Quest for
1443 Competition and Ecological Niche Differentiation.” *Journal of Bioscience and Bioengineering*
1444 123 (5): 581–89. <https://doi.org/10.1016/j.jbiosc.2016.12.016>.

1445 Vaccaro, Ralph F., and John H Ryther. 1960. “Marine Phytoplankton and the Distribution of Nitrite in
1446 the Sea*.” *ICES Journal of Marine Science* 25 (3): 260–71.
1447 <https://doi.org/10.1093/icesjms/25.3.260>.

1448 Vajjala, Neeraja, Willm Martens-Habbena, Luis A. Sayavedra-Soto, Andrew Schauer, Peter J.
1449 Bottomley, David A. Stahl, and Daniel J. Arp. 2013. “Hydroxylamine as an Intermediate in
1450 Ammonia Oxidation by Globally Abundant Marine Archaea.” *Proceedings of the National*
1451 *Academy of Sciences of the United States of America* 110 (3): 1006–11.
1452 <https://doi.org/10.1073/pnas.1214272110>.

1453 Volk, T., and M. I. Hoffert. 1985. “Ocean Carbon Pumps: Analysis of Relative Strengths and
1454 Efficiencies in Ocean-Driven Atmospheric CO₂ Changes.” *The Carbon Cycle and Atmospheric*
1455 *CO₂*.

1456 Walker, C. B., J. R. De La Torre, M. G. Klotz, H. Urakawa, N. Pinel, D. J. Arp, C. Brochier-Armanet,
1457 et al. 2010. “Nitrosopumilus Maritimus Genome Reveals Unique Mechanisms for Nitrification
1458 and Autotrophy in Globally Distributed Marine Crenarchaea.” *Proceedings of the National*
1459 *Academy of Sciences of the United States of America* 107 (19): 8818–23.
1460 <https://doi.org/10.1073/pnas.0913533107>.

1461 Ward, B. B. 2005. “Temporal Variability in Nitrification Rates and Related Biogeochemical Factors
1462 in Monterey Bay, California, USA.” *Marine Ecology Progress Series* 292: 97–109.
1463 <https://doi.org/10.3354/meps292097>.

1464 ———. 2008. “Chapter 5 - Nitrification in Marine Systems.” In *Nitrogen in the Marine Environment*
1465 *(2nd Edition)*, 199–261. <https://doi.org/http://dx.doi.org/10.1016/B978-0-12-372522-6.00005-0>.

1466 Ward, B. B., and K. A. Kilpatrick. 1991. “Nitrogen Transformations in the Oxidic Layer of Permanent
1467 Anoxic Basins: The Black Sea and the Cariaco Trench.” In *Black Sea Oceanography*.
1468 https://doi.org/10.1007/978-94-011-2608-3_7.

1469 Ward, B. B., and O. C. Zafriou. 1988. “Nitrification and Nitric Oxide in the Oxygen Minimum of the
1470 Eastern Tropical North Pacific.” *Deep Sea Research Part A, Oceanographic Research Papers*
1471 35 (7): 1127–42. [https://doi.org/10.1016/0198-0149\(88\)90005-2](https://doi.org/10.1016/0198-0149(88)90005-2).

1472 Watson, Andrew J., Ute Schuster, Jamie D. Shutler, Thomas Holding, Ian G.C. Ashton, Peter
1473 Landschützer, David K. Woolf, and Lonneke Goddijn-Murphy. 2020. “Revised Estimates of
1474 Ocean-Atmosphere CO₂ Flux Are Consistent with Ocean Carbon Inventory.” *Nature*
1475 *Communications* 11 (1): 1–6. <https://doi.org/10.1038/s41467-020-18203-3>.

1476 Watson, Stanley W., Eberhard Bock, Frederica W. Valois, John B. Waterbury, and Ursula Schlosser.
1477 1986. “Nitrospira Marina Gen. Nov. Sp. Nov.: A Chemolithotrophic Nitrite-Oxidizing
1478 Bacterium.” *Archives of Microbiology*. <https://doi.org/10.1007/BF00454947>.

1479 Watson, Stanley W., and John B. Waterbury. 1971. "Characteristics of Two Marine Nitrite Oxidizing
1480 Bacteria." *Microscopy* 77 (2631): 203–30.

1481 Weigand, M. Alexandra, Julien Foriel, Bruce Barnett, Sergey Oleynik, and Daniel M. Sigman. 2016.
1482 "Updates to Instrumentation and Protocols for Isotopic Analysis of Nitrate by the Denitrifier
1483 Method." *Rapid Communications in Mass Spectrometry* 30 (12): 1365–83.
1484 <https://doi.org/10.1002/rcm.7570>.

1485 Xu, Min Nina, Xiaolin Li, Dalin Shi, Yao Zhang, Minhan Dai, Tao Huang, Patricia M. Glibert, and
1486 Shuh Ji Kao. 2019. "Coupled Effect of Substrate and Light on Assimilation and Oxidation of
1487 Regenerated Nitrogen in the Euphotic Ocean." *Limnology and Oceanography* 64 (3): 1270–83.
1488 <https://doi.org/10.1002/lno.11114>.

1489 Yool, Andrew, Adrian P Martin, Camila Fernández, and Darren R Clark. 2007. "The Significance of
1490 Nitrification for Oceanic New Production." *Nature* 447 (7147): 999–1002.
1491 <https://doi.org/10.1038/nature05885>.

1492 Zakem, Emily J., Alia Al-Haj, Matthew J. Church, Gert L. Van Dijken, Stephanie Dutkiewicz, Sarah
1493 Q. Foster, Robinson W. Fulweiler, Matthew M. Mills, and Michael J. Follows. 2018.
1494 "Ecological Control of Nitrite in the Upper Ocean." *Nature Communications* 9 (1).
1495 <https://doi.org/10.1038/s41467-018-03553-w>.

1496 Zhang, Yao, Wei Qin, Lei Hou, Emily J. Zakem, Xianhui Wan, Zihao Zhao, Li Liu, et al. 2020.
1497 "Nitrifier Adaptation to Low Energy Flux Controls Inventory of Reduced Nitrogen in the Dark
1498 Ocean." *Proceedings of the National Academy of Sciences of the United States of America* 117
1499 (9): 4823–30. <https://doi.org/10.1073/pnas.1912367117>.

1500
1501
1502
1503
1504
1505
1506
1507
1508
1509
1510
1511
1512
1513
1514
1515
1516
1517

1518 **Tables and figures**

1519 **Table 1:** Kinetic parameters (V_{\max} , K_m , and C) associated with NO_2^- oxidation experiments conducted
 1520 across the western Indian sector of the Southern Ocean in winter 2017. Included here is the best fit and
 1521 95% confidence interval ("CI") for each kinetic parameter, derived using a non-linear, least-squares
 1522 optimization method (Scipy lmfit package, Python 3.7.6).

Table 1

Station name	Latitude	Longitude	$[\text{NO}_2^-]_{\text{amb}}$ (nM)	V_{\max} (nM d ⁻¹)	95%CI (nM d ⁻¹)	K_m (nM)	95%CI (nM)	C (nM)	95%CI (nM)
St 01	37°S	19°E	157	9.1	7.9 to 10	263	192 to 350	193	144 to 206
St 02	42°S	21°E	108	5.2	4.8 to 5.5	134	109 to 163	115	105 to 119
St 03	45°S	22°E	103	8.3	7.4 to 9.3	206	15 to 373	139	-11 to 163
St 04	50°S	26°E	162	13	11 to 15	288	104 to 538	172	68 to 204
St 05	55°S	28°E	212	14	13 to 15	329	183 to 458	245	138 to 272
St 06	62°S	30°E	226	8.2	7.8 to 8.6	403	320 to 499	163	129 to 187
St 07	62°S	30°E	226	6.6	6.0 to 7.4	317	234 to 395	237	190 to 255

1523
 1524 **Table 2:** A selection of previously derived K_m and V_{\max} values from the open ocean, along with the
 1525 concurrently-measured ambient concentrations of nitrite ($[\text{NO}_2^-]_{\text{amb}}$). The numbers in parenthesis are
 1526 standard errors.

Table 2

Region	$[\text{NO}_2^-]$ (nM)	Sampled depth (m)	K_m (nM)	V_{\max} (nM d ⁻¹)	Reference
Indian Southern Ocean: St 01: 37°S	157	7	263 (16)	9.1 (0.5)	This study
Indian Southern Ocean: St 02: 42°S	108	7	134 (8)	5.2 (0.1)	This study
Indian Southern Ocean: St 03: 45°S	103	7	206 (30)	8.3 (0.4)	This study
Indian Southern Ocean: St 04: 51°S	162	7	288 (52)	13 (0.7)	This study
Indian Southern Ocean: St 05: 56°S	212	7	329 (29)	14 (0.4)	This study
Indian Southern Ocean: St 06: 62°S	226	7	403 (24)	8.2 (0.1)	This study
Indian Southern Ocean: St 07: 62°S	226	7	317 (20)	6.6 (0.3)	This study
Southern California Bight	20	60	70	nd	Olson 1981
Eastern Tropical North Pacific	100	53	281 (151)	63 (14)	Sun et al. 2017
Eastern Tropical North Pacific	50	170	227 (55)	56 (5.4)	Sun et al. 2017
South China Sea	51	110	195 (33)	30 (1.6)	Zhang et al. 2020
South China Sea	71	95	175 (37)	24 (1.5)	Zhang et al. 2020
South China Sea	31	150	49 (15)	9.6 (0.6)	Zhang et al. 2020
South China Sea	185	75	506 (82)	12 (0.8)	Zhang et al. 2020
South China Sea	34	200	27 (11)	4.6 (0.3)	Zhang et al. 2020
Subtropical South Atlantic	14	150	74 (29)	22 (0.7)	Fawcett et al. unpubl.
Subtropical South Atlantic	152	150	167 (4.3)	27 (0.2)	Fawcett et al. unpubl.

nd represents not determined

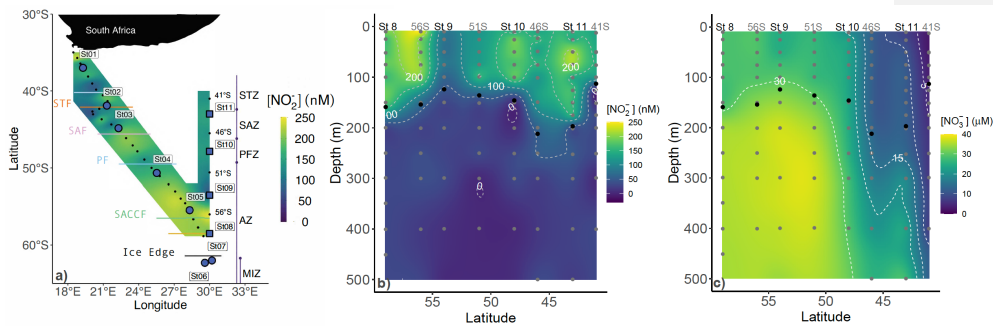
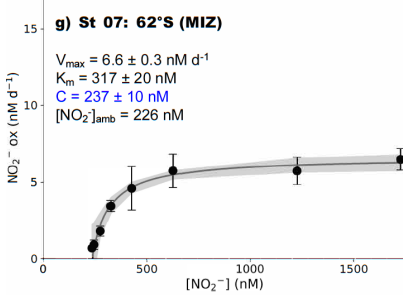
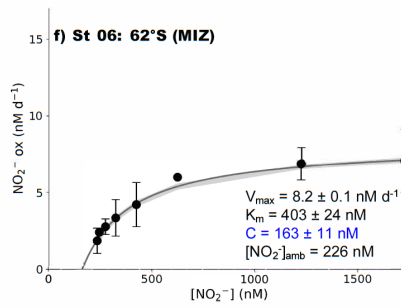
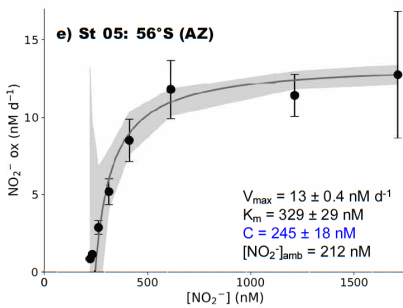
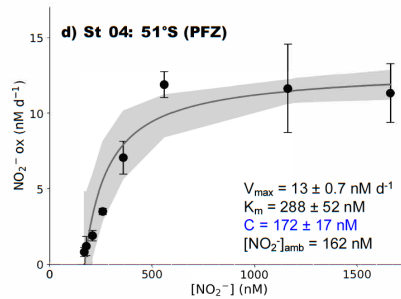
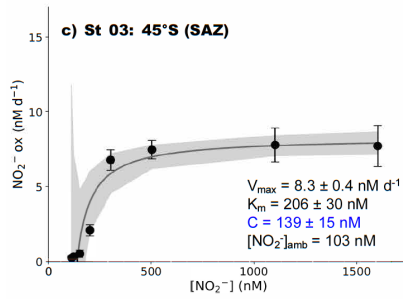
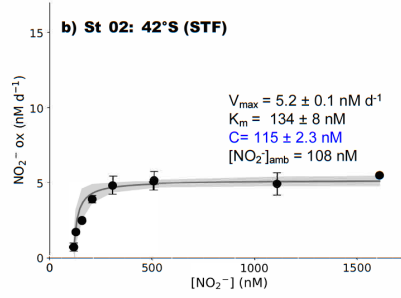
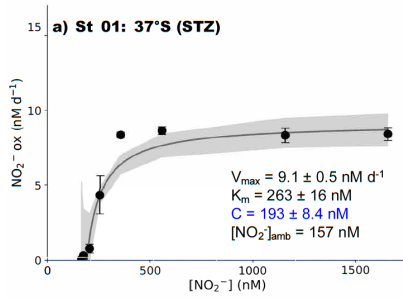


Figure 1: a) Map of the cruise track showing the kinetics stations (large circle symbols) and locations of the underway stations sampled during Leg 1 (small symbols), overlaid on the measured surface (~7 m) nitrite concentrations ($[\text{NO}_2^-]$). Additionally, the locations of the hydrocast stations occupied during Leg 2 are shown, with the stations at which depth-profile experiments were conducted shown by the large square symbols. The coloured horizontal lines denote the frontal positions at the time of sampling and the major zones of the Southern Ocean are indicated by the vertical lines and dots – STZ, Subtropical Zone; STF, Subtropical Front; SAZ, Subantarctic Zone; SAF, Subantarctic Front; PFZ, Polar Frontal Zone; PF, Polar Front; AZ, Antarctic Zone; SACCF, Southern Antarctic Circumpolar Front; MIZ, Marginal Ice Zone. Also shown are water column (0-500 m) profiles of the concentrations of b) nitrite (NO_2^-) and c) nitrate (NO_3^-) sampled during Leg 2. The grey dots indicate the discrete sampling depths at all the hydrocast stations (eight in total), with the four stations at which depth profile experiments were conducted (St 08 to St 11) labeled above the panel. The black dots show the derived mixed layer depths.

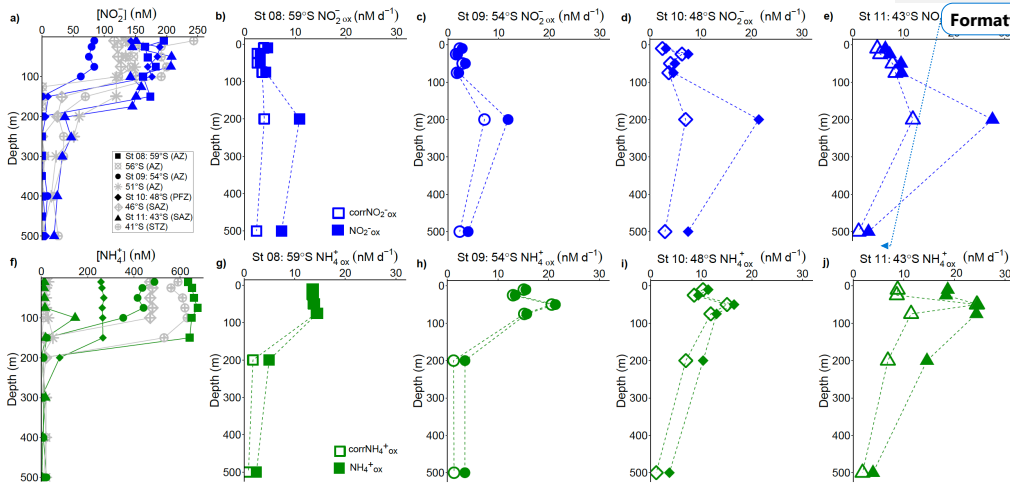


1544 **Figure 2:** Kinetics experiments: the dependence of the NO_2^- oxidation rates on NO_2^- concentration
 1545 ($[\text{NO}_2^-]$) at the surface (~ 7 m) in winter at a) St 01: 37°S (STZ), b) St 02: 42°S (STF), c) St 03: 45°S
 1546 (SAZ), d) St 04: 51°S (PFZ), e) St 05: 55°S (OAZ), f) St 06: 62°S (MIZ), and g) St 07: 62°S (MIZ).
 1547 The solid lines show the Michaelis-Menten best fit, with the derived values of V_{max} , K_m , and C , as well
 1548 as the ambient concentration of nitrite ($[\text{NO}_2^-]_{\text{amb}}$), indicated on each panel. Error bars represent the
 1549 range of values, each measured at least twice. Where error bars are not visible, they are smaller than
 1550 the data markers. The grey shaded area shows the 95% confidence interval associated with the model
 1551 fit. Note that the x-axis represents total $[\text{NO}_2^-]$ (i.e., $[\text{NO}_2^-]_{\text{tracer}} + [\text{NO}_2^-]_{\text{amb}}$).

Deleted: show

Deleted: standard error

Deleted: of replicate experiments



Formatted: Centred

1554 **Figure 3:** Depth-profile experiments: water column (0-500 m) profiles of the concentration of a) nitrite
 1555 ($[\text{NO}_2^-]$) and f) ammonium ($[\text{NH}_4^+]$), and rates of NO_2^- and NH_4^+ oxidation at b and g) St 08: 59°S (AZ),
 1556 c and h) St 09: 54°S (AZ), d and i) St 10: 48°S (PFZ), and e and j) St 11: 43°S (SAZ). In panels a and
 1557 f, the blue and green symbols indicate the stations at which oxidation rates were measured while the
 1558 grey symbols show data from the stations where no experiments were conducted. In panels b-e and g-
 1559 j, open symbols show the oxidation rates revised for possible stimulation due to ^{15}N -tracer additions
 1560 ($\text{corrNO}_2^-_{\text{ox}}$ and $\text{corrNH}_4^+_{\text{ox}}$; equation 4) and closed symbols show the uncorrected rates (equation 1).
 1561 Error bars indicate the range of values, each measured at least twice. Where error bars are not visible,
 1562 they are smaller than the data markers. The dashed lines connecting the data points are included only to
 1563 guide the eye and should not be taken to imply interpolation with depth.

Deleted: standard error of replicate experiments

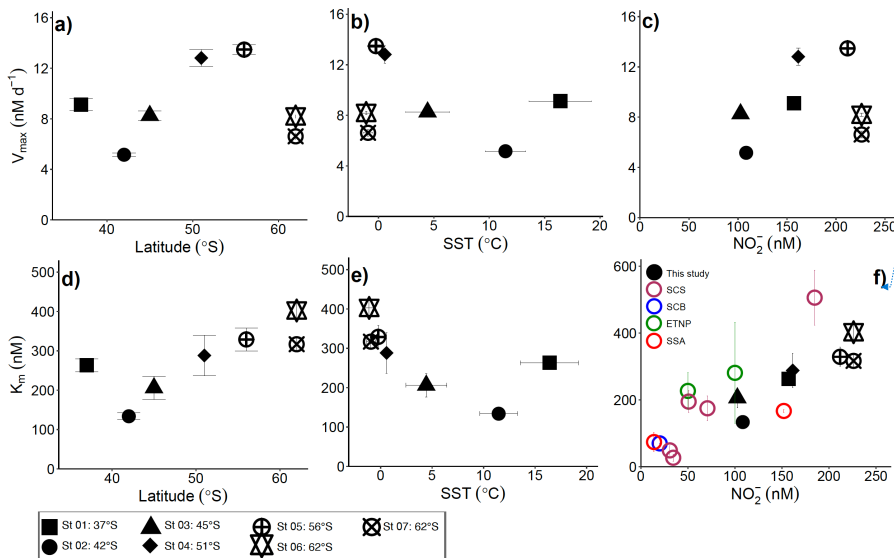


Figure 4: Potential controls on the kinetic parameters associated with NO_2^- oxidation. V_{\max} and K_m are shown as a function of a and d) latitude, b and e) sea surface temperature (SST), and c and f) the ambient nitrite concentration ($[\text{NO}_2^-]_{\text{amb}}$). Vertical error bars show the propagated error associated with V_{\max} and K_m computed using a non-linear, least-squares optimization method (Scipy lmfit package, Python 3.7.6), while the symbols and horizontal error bars on panels b and e indicate the average (± 1 standard deviation) SST experienced by the sampled communities during the incubations. In panel f, black symbols show our Southern Ocean data, maroon symbols show K_m values from the South China Sea (SCS; Zhang et al. 2020), the blue symbol shows the K_m value derived for the South California Bight (SCB; Olson 1981a), the green symbol shows K_m values from Eastern Tropical North Pacific oxygen deficient zone (ETNP; Sun et al. 2017), and the red symbols show K_m values derived for the subtropical southeast Atlantic (SSA; Fawcett et al. unpubl.).

Formatted: Centred

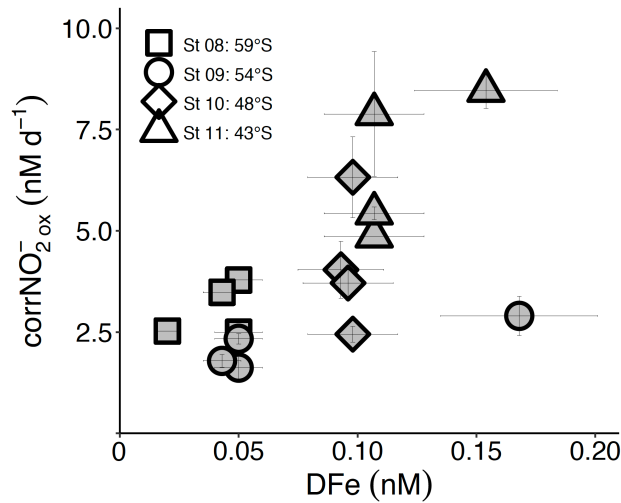


Figure 5: Euphotic zone (0-75 m) revised rates of NO_2^- oxidation ($\text{corrNO}_2^-_{\text{ox}}$) measured at the depth-profile stations (St 08 to St 11) plotted against coincident dissolved iron concentrations (DFe). Error bars indicate the [range of values](#), each measured at least twice. Where errors bars are not visible, they are smaller than the data markers.

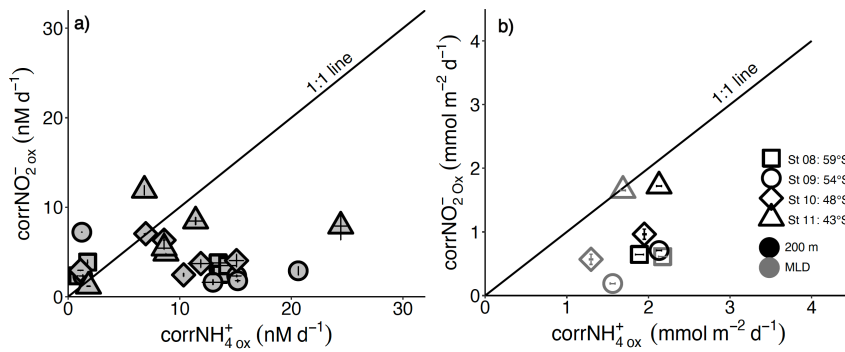


Figure 6: The relationship between the revised rates of NO_2^- and NH_4^+ oxidation ($\text{corrNO}_2^-_{\text{ox}}$ and $\text{corrNH}_4^+_{\text{ox}}$) for a) each experiment depth in the upper water column (0-500 m) and b) integrated over the mixed layer (grey symbols) and upper 200 m (black symbols). Error bars on panel a indicate the [range of values](#), each measured at least twice, while on panel b, error bars show the propagated error. Where errors bars are not visible, they are smaller than the data markers. The black diagonal line on both panels has a slope of 1, which is expected if the rates of NH_4^+ and NO_2^- oxidation are tightly coupled.

Formatted: Centred

Deleted: standard error of replicate experiments/collections

Formatted: Centred

Deleted: standard error of replicate experiments

